CHAPTER FOUR

Antiphospholipid Syndrome: Mechanisms Revealed in Erythrocyte and Liposome Studies

Snežna Sodin-Šemrl,[1,*] Blaž Rozman,[1] Aleš Iglič,[2] *and* Veronika Kralj-Iglič[3]

Contents

Abstract

The loss of membrane asymmetry is an important feature in mechanisms involved in maintaining immunity. Negatively charged phospholipids are present only in small amounts in the outer leaflet of the membranes of viable cells. In some pathological conditions and in apoptosis, negatively charged phospholipids become exposed on the

* Corresponding author. Tel.: +386 1 5225596; Fax: +386 1 5225598;
E-mail address: snezna.sodin@kelj.si (S. Sodin-Semrl).

[1] Department of Rheumatology, University Medical Center, Vodnikova 62, SI-1000 Ljubljana, Slovenia
[2] Laboratory of Physics, Faculty of Electrical Engineering, University of Ljubljana, Tržaška 25, SI-1000 Ljubljana, Slovenia
[3] Laboratory of Clinical Biophysics, Faculty of Medicine, University of Ljubljana, Lipičeva 2, SI-1000 Ljubljana, Slovenia

Advances in Planar Lipid Bilayers and Liposomes, Volume 7
ISSN 1554-4516, DOI: 10.1016/S1554-4516(08)00004-5

outer membrane surface facing among other surroundings, the blood plasma. There, they can contribute to the catalytic potential for chemical reactions leading to blood clot formation. Also, they serve, in connection with protein cofactors, as antigens in the immune system leading to autoantibody formation and autoimmune diseases, among them of special emphasis, antiphospholipid syndrome (APS).

APS is manifested clinically by venous and arterial thromboses and fetal loss. Laboratory analysis reveals a presence of antiphospholipid antibodies (aPL) in the patients' blood and research analysis indicates an increased amount of cell-derived microvesicles (MVs). MVs often have an impaired membrane asymmetry and can be procoagulant. Elevation of MV quantity in patient sera from different cells has been shown to be associated with thromboses. It is indicated that MVs can also be antigenic, depending on the properties and content of the blood plasma, that is, the presence in plasma of certain proteins called protein cofactors. Although numerous methods have been used in attempt to understand the antigen–phospholipid–antibody interactions and their role in APS, knowledge of the underlying mechanisms remains fragmentary. In this chapter, we study complex interactions between protein cofactors, phospholipid membranes, and aPL in giant phospholipid vesicles and in erythrocytes. We consider the process of budding and vesiculation in giant phospholipid vesicles and in erythrocytes, plasma protein-mediated attraction of negatively charged phospholipid membranes, and effects of annexin A5 (ANXA5) on interaction of protein cofactors and aPL with the phospholipid membranes. Our results indicate that phospholipid vesicles and erythrocytes can be useful not only in elucidating basic mechanisms involved in APS but can serve as models of antigen–phospholipid–antibody interactions with potential for improving clinical diagnosis and/or prognosis of this debilitating and sometimes lethal autoimmune disorder. Further studies in this direction should be undertaken.

1. Introduction

Antiphospholipid syndrome (APS) is a rather new clinical entity known since 1983 when definite recognition of APS started with the introduction of sensitive solid phase assays of anticardiolipin antibodies (aCL) [1]. Clinical criteria encompass vascular thrombosis and pregnancy morbidity. Laboratory criteria include the presence of lupus anticoagulants (LA) in plasma and antiphospholipid antibodies (aPL) in serum and plasma. Early studies of the mechanisms involved in APS focused on the interactions between phospholipids and antibodies, until the 1990s, when the first protein cofactor, that is, β2-glycoprotein I (β2GPI) was determined as antigenic [2–4]. It is now acknowledged that the antigenic targets of aPL in ELISA tests are not the phospholipids themselves, but plasma protein cofactors, such as β2GPI, prothrombin (PT), and annexin A5 (ANXA5), interacting with phospholipid surfaces [5–7].

One of the processes underlying both thrombosis and the autoimmune response is microexovesiculation of the cell membrane which is the final event in the process of membrane budding. Microexovesicles (also called microparticles) enter the circulation and may convey material and information to distant cells. They have been recognized to play an important role in thrombosis, inflammation, and promotion of cancer [8–11]. In particular, increased levels of MVs were found in patients with APS [12].

In spite of numerous biochemical studies, a decisive answer concerning the role of protein cofactors and antiphosphoplipid antibodies in the pathogenesis of APS has not yet been given. The study of physical mechanisms should be undertaken to complement the study of biochemical aspects. In this regard, microvesiculation represents a promising subject worthy to be further explored. It is of particular interest to study the role of phospholipids, protein cofactors, and antibodies in the process of membrane vesiculation and propose possible mechanisms of their role in related clinical manifestations.

There is a continuous search for appropriate *in vitro* models of biological cells. Erythrocytes and giant phospholipid vesicles have been proven useful due to lack of internal structure and sufficient size for observation under the light microscope. In these systems, the budding and vesiculation of the membrane can be induced by different trigger mechanisms in the presence or absence of the protein cofactors and antibodies in the surrounding solution. We believe that elucidating these processes would help in understanding protein–protein and protein–lipid interactions underlying the clinical manifestations of thrombosis and/or fetal loss in APS patients.

2. Biochemical Aspects of Mechanisms Involved in APS

In this section, we describe the key factors involved in APS and their possible roles in corresponding biochemical mechanisms, in particular in interaction with membranes including negatively charged phospholipids. The most thoroughly studied molecules involved in APS are phospholipids [cardiolipin (CL) and phosphatidylserine (PS)], protein cofactors (β2GPI, PT, and ANXA5), and their antibodies.

2.1. Exposure of Negatively Charged Membrane Surfaces due to Loss of Membrane Asymmetry and Its Role in APS

One of the major mechanisms implicated in the development of immunogenicity against phospholipids such as CL, PS, and their protein cofactors is the loss of membrane phospholipid asymmetry. The outer membrane leaflet of eukaryotic cells is formed predominantly with cholinephospholipids (such as phosphatidylcholine, sphingomyelin, and glycosphingolipids) whereas the inner (cytoplasmic) leaflet is composed predominantly of aminophospholipids such as phosphatidylethanolamine [13]. Other phospholipids of minor abundance, such as phosphatidic acid and phosphatidylinositol are located in the inner leaflet. Human erythrocytes normally comprise of less than 4% PS in the outer leaflet of the membrane [14], whereas human platelets have a slightly higher PS content [14, 15]. Virtually every cell in the body restricts PS to the inner leaflet of the plasma membrane by an energy-dependent transport from the outer to the inner leaflet of the bilayer [16]. The loss of transmembrane phospholipid asymmetry, with consequent exposure of PS in the external monolayer occurs both in normal and pathologic conditions. PS distributes to the outer leaflet during cell activation and apoptosis involving flippase,

floppase, and scramblase enzymes [17]. The flippase enzyme activity is highly selective for PS and functions to keep this lipid sequestered from the cell surface [18].

Loss of this asymmetry is associated with many physiological states, in addition to apoptosis, such as cell activation, clearance, and senescence, as well as with pathological conditions such as thrombosis and tumorigenesis [19, 20]. The translocation of CL, which is normally located on the inner mitochondrial membrane, to plasma membranes (as is the case with PS) also appears to occur in apoptosis. While the process of PS exposure can occur within seconds, the exposure of CL is slower as it must traverse multiple membranes.

2.2. Cardiolipin

CL is a phospholipid located predominantly in energy transducing membranes such as mammalian inner mitochondrial membranes where it plays a role in many multimeric complexes associated with these membranes. CL differs from all other phospholipids in that it has four acyl chains and a dimeric headgroup which carries at physiologic pH two negative charges. CL rapid remodeling into highly unsaturated species (tetra-linoleyl-CL) most commonly found in adult tissues, involves relocation to other membranes (outer mitochondrial membrane and extra-mitochondrial membranes) [21]. CL and its metabolites, such as monolyso-CL (MCL), dilyso-CL (DCL), and hydro-CL move from mitochondria to other cellular membranes during death receptor-mediated apoptosis where CL exhibits segregation. The chemistry of CL acyl chains is important for both the binding to β2GPI as well as for the intrinsic immunogenicity of the CL molecule [21]. The CL degradation process occurs in both, membranes of the mitochondria as part of remodeling mature lipids, and in lysosomes as well. CL is one of the most resistant phospholipids (against phospholipase A2 hydrolysis) in membranes of healthy cells. Some MCL exist also in healthy tissue; however, their abundance increases significantly in response to apoptotic stimuli. β2GPI shows a differential binding to CL derivatives (with highest binding to MCL $>$ CL $>$ DCL). The degree of unsaturation of acyl chains in CL influences the binding of β2GPI to CL and (hydro)peroxidation of CL is essential for enhancing the binding of aPL [22]. CL hydrolysis of one fatty acid chain could yield MCL to enhance CL antigenicity. MCL has hybrid properties between a diacyl-lipid (bilayer forming) and a lyso-lipid (micelle forming) form, which also may facilitate autoantibody reactivity [21]. The loss of an acyl chain in DCL and an unusually large and hydrophilic polar head could destroy the binding affinity of this CL metabolite for β2GPI. It is therefore indicated that probable links exist between apoptotic changes, oxidative states, CL metabolism, generation of CL derivatives, and the recognition and production of aCL antibodies. Leakage of CL and its exposure on cell surfaces precede DNA fragmentation, so CL localization to the plasma membrane represents an early event of apoptosis and may be a trigger of aCL development [23].

At physiologic Ca^{++} cytoplasmic concentrations, both the translocase (flippase) and floppase are active generating and maintaining phospholipid asymmetry. The lipid scramblase activity, however, can lead to the collapse of the membrane asymmetry, especially in conditions of high Ca^{++} when the scramblase is activated

and the actions of translocase (flippase) and floppase are blocked, a condition leading to loss of asymmetry and having the consequence of cells being primed for pathological events, such as autoimmune antibody development. Subang *et al.* [24] confirmed this hypothesis by showing that β2GPI bound to anionic phospholipids (that may be expressed on the surface of apoptotic cells), was immunogenic. The group immunized BALB/C mice with β2GPI in the presence of CL or PS vesicles. CL vesicles induced the highest levels of anti-β2GPI and aCL IgG antibodies. Alessandri *et al.* [21] demonstrated that a critical number of acyl chains in CL derivates is important for binding of aPL and that MCL is one of the antigenic targets with immunoreactivity comparable to CL in APS and systemic lupus erythematosus. IgG fractions from APS patients were used to analyze the distribution pattern of CL and its derivatives on the surface of apoptotic endothelial cells (HUVEC). Stronger binding of IgG fractions were observed to apoptotic HUVEC than to nonapoptotic, untreated cells. β2GPI has a strong affinity for PS, phosphatidic acid, and CL and has been previously reported not to bind to neutral phospholipids, such as PC, phosphatidylethanolamine, and sphingomyelin [21].

2.2.1. Antibody characterization

It is generally agreed that the term aCL, if not stated otherwise, defines the antibodies against CL detected by the classical aCL ELISA as both, β2GPI independent as well as β2GPI dependent. Even though this method is standardized [25], there is variation between the tests.

2.2.2. Clinical significance

aCL as detected by the classical ELISA are not only believed to be markers of thrombosis occurring in APS and other autoimmune diseases, but also occasionally show an association with other diseases, especially infections. Infectious aCL usually disappear from patient sera in less than three months.

2.3. Phosphatidylserine

A critical role for PS in thrombosis was suggested by Bevers *et al.* [26, 27] who reported that the asymmetric orientation of phospholipids in blood platelets was rapidly lost during their activation following an influx of Ca^{++}. This points to the involvement of the enzyme lipid scramblase, which requires a continuous presence of cytoplasmic calcium, in moving all classes of lipids bidirectionally. Without the action of lipid scramblase, lipids of the platelet plasma membrane would flip-flop resulting in a loss of membrane asymmetry within minutes. When proteins fractionated from such platelet membranes were reconstituted into artificial lipid vesicles, they exhibited Ca^{++}-dependent lipid scrambling activity that was pronase-, heat-, and sulfhydryl sensitive [28]. Other consequences of PS presence in the outer leaflet of membranes include among others: formation of a procoagulant surface following platelet activation [14], early detection of apoptosis [16], and high adherence of damaged erythrocytes (sickled cells or ghosts) to endothelial cells. There was an accelerated clearance of damaged cells by monocytes and macrophages. This mechanism of recognition could be responsible for the elimination of aged erythrocytes

from the bloodstream. Failure to efficiently remove apoptotic cells may contribute to inflammatory responses and autoimmune diseases resulting from chronic exposure of PS. It is interesting that non-apoptotic PS externalization is induced by several activation stimuli, including engagement of immunoreceptors [29]. Unregulated loss of PS asymmetry may contribute significantly to heart disease and stroke [16].

2.3.1. Antibody characterization

Anti-PS antibodies (anti-PS) have been mainly studied in connection with different protein cofactors, such as PT and β2GPI.

2.3.2. Clinical significance

In autoimmune diseases, anti-PS can sometimes be detected independently from aCL [30]. It has also been indicated that anti-PS destroy human trophoblasts, halt human chorionic gonadotropin production, and limit trophoblast invasion [31].

2.4. Protein Cofactors and Their Antibodies

2.4.1. β2-Glycoprotein I

β2GPI is a 50-kDa protein as estimated by denaturing polyacrylamide gel electrophoresis and represents a major autoantigen for the production of aPL shown to be involved in autoimmune diseases, such as APS. The human β2GPI 326 amino acid sequence was determined from purified protein [32] and the entire single chain polypeptide has extensive internal homology within its five consecutive 60 amino acid homologous sushi domains. The crystal structure of β2GPI has been resolved and reveals a J-shaped structure with four aligned segments and a fifth structurally different segment with an additional hydrophobic lysine rich loop thought to insert into the phospholipid membrane [33]. The lysine rich loop, located between Cys 281-Cys 288 of the fifth β2GPI domain [34], is held responsible for electrostatic interactions between the positively charged patch in domain five and anionic phospholipid headgroups [35]. Insertion of this lysine rich loop into the phospholipid membrane was found to be necessary for vesicles and cell membrane fragments to be cleared from the circulation [36]. The three-dimensional structure of a typical domain has a hydrophobic core containing conserved residues bordered on either side by small anti-parallel β-pleated sheets. Each domain has two disulfide bonds, with the exception of the fifth which has three. β2GPI is highly glycosylated, with five attached glucosamine-containing oligosaccharides, located in domains III and IV, the variability of which is thought to account for at least five isoforms as judged by isoelectric focusing [37]. Glycosylation influences the conformation and antibody binding, but does not affect the β2GPI binding capacity to lipid membranes [38, 39]. β2GPI is presumed to undergo the sorting and targeting transit through the Golgi apparatus after initial synthesis in the rough endoplasmic reticulum. There are no studies to date describing β2GPI mutation effects on localization, or degradation. It has been shown that β2GPI also plays a role in the modulation of triacylglycerol-rich lipoprotein metabolism [40], atherogenesis [41], and atherosclerosis [42, 43]. *In vitro* studies have shown β2GPI to be an anti-coagulant factor involved in mechanisms such as inhibition of the coagulation pathway [44], platelet prothrombinase

activity [45], and platelet aggregation [46], all of which propose a protective role in the pathogenesis of thrombosis. There have been reports, however, describing the role of β2GPI in potentially pro-coagulant activities such as inhibition of activated protein C anti-coagulant activity [47] and its ability to bind monocyte surface and promote tissue factor expression [48]. This latter binding required the presence of aPL.

Putative receptors for β2GPI have been identified in HUVEC [49, 50], renal epithelial cells [51], and platelets [52]. When macrophages fail to maintain their membrane lipid asymmetry, β2GPI has been shown to bind PS [53]. The binding of β2GPI to HUVEC is of high affinity ($K_d = 18$ nM) and has been shown to be specifically mediated by annexin 2 [49]. Endothelial cell activation by anti-β2GPI antibodies has been indicated to be due to binding with β2GPI likely associated with one or more toll-like receptors [50] causing proadhesive and proinflammatory responses. In the kidneys, β2GPI has been suggested to be a cell recognition mediator for PS exposing particles. An efficient and physiologically relevant receptor for β2GPI has been identified in renal epithelial cells to be megalin, which following interaction with β2GPI, mediates endocytosis and renal clearance. β2GPI bound to PS and CL shows an increased affinity for megalin [51]. Recently, an additional receptor has been identified as apolipoprotein E receptor 2′ which has been shown to be involved in activation of platelets by dimeric β2GPI [52].

2.4.1.1. Antibody characterization β2GPI is known to bind not only to negatively charged phospholipids in artificial systems but also to surface membranes of cells directly involved in the pathogenic mechanism of APS, such as activated or apoptosing cells (platelets, endothelial cells). There is a lack of information which would unite crucial data necessary in order to determine whether negatively charged phospholipids are essential for both activation and apoptotic signaling to occur. The proposed mechanism of platelet activation is dependent on the dimerization of β2GPI by aPL. This binding stabilizes the complex on the surface of platelets leading to a stronger adhesion of β2GPI-aPL to phospholipids [52]. β2GPI binding to HUVEC cells lead to exposed epitopes which can be recognized by circulating anti-β2GPI antibodies, which stimulate induction of cell activation, triggering prothrombotic events, contributing to the hypercoagulable state of APS patients [54]. The proposed function and consequence of aPL binding to phospholipid bound β2GPI on either monocytes or endothelial cells elicits p38 MAP kinase phosphorylation, leading to translocalization of NF-kB into the nucleus and transcription of procoagulant factors, such as tissue factor, plasminogen activator inhibitor-1, tumor necrosis factor alpha, and endothelin-1 [55, 56]. β2GPI also binds to sulfatides (acidic glycosphingolipids with sulfate esters on oligosaccharide chains) at physiological concentrations and these complexes are recognized by antibodies from patients with APS [57].

Anti-β2GPI either recognize conformational and cryptic epitopes on β2GPI after binding to phospholipid membranes or bivalently bind to β2GPI molecules in close proximity [5]. Anti-β2GPI are generally believed to be of low avidity and bind only to high density of β2GPI molecules on phospholipid membranes. Recently it was shown that neither high density of the antigen nor high avidity of the antibodies (or Fab fragments) alone was sufficient for the binding of anti-β2GPI to its antigen.

Some conformational modifications and consequently, exposed neoepitopes are required for the recognition of β2GPI by polyclonal anti-β2GPI [58].

2.4.1.2. Clinical significance Anti-β2GPI antibodies are an independent risk factor for thrombosis [59, 60] and pregnancy complications [61, 62], even though some studies deny these associations mainly because of methodological differences and lack of standardization [63]. In meta-analyses of 20 studies, anti-β2GPI antibodies seemed to be more often associated with venous thrombosis as compared to arterial events [59].

2.4.2. Prothrombin

PT is an approximately 72 kDa glycoprotein synthesized in the liver, secreted into circulation and present at $\sim$100 μg/ml concentrations in normal plasma. Posttranslationally PT undergoes carboxylation of its glutamic residues, known as the GLA domain, which is essential for the Ca^{++}-dependent binding of phospholipid to PT. The GLA domain is followed by the two Kringle domains responsible for interaction with substrate–cofactor receptors [64, 65]. PT is unique among the activated coagulation proteinases in that it completely loses the domains important for initial recognition interactions when it is activated to its serine proteinase derivative, thrombin [66]. PT is activated at sites of vascular injury to yield its active form thrombin. Thrombin is generated by cleavage to yield a F1 + 2 fragment containing GLA and two Kringle domains, which originally function to localize PT on membrane surfaces as part of the activation complex, that includes factor Va and factor Xa. Because it loses its F1 + 2 fragment, thrombin's determinants for substrate recognition remain on its catalytic domain. Thrombin is one of the most studied major enzymes involved in many stages of blood coagulation and platelet aggregation, fibrinogen cleavage, and fibrin clot formation. Antibodies against PT are postulated to dysregulate some of these processes [66].

2.4.2.1. Antibody characterization There are two types of anti-PT antibodies able to be detected. anti-PT can be evaluated by utilizing either human PT directly coated onto ELISA plates or complexed with PS, neither of which is standardized. anti-PT bind to PT coated on irradiated or high-activated polyvinylchloride, but not on plain polystyrene ELISA plates. IgG and/or IgM antibodies to human PT in solid phase have been reported in approximately half of the patients with aPL. PT is recognized more efficiently when the protein is bound to PS-coated ELISA plates using calcium ions. Multiple explanations could account for this. The first one considers that PT complexed to PS is not likely to be restricted in its lateral movements; this would allow clustering and proper orientation, offering better binding conditions for the antibodies. The second alternative considers that the circulating PT-anti-PT immune complexes present in some samples may be captured on ELISA with PS. The third alternative is that anti-PT might react with neoepitopes that PT makes available only when bound to PS through calcium ions [67]. Recent evidence from Rauch *et al.* [68] indicates that anti-PT recognize PT also when bound to hexagonal phase phosphatidylethanolamine and that the plasma LA activity is

specifically neutralized by the prothrombin/hexagonal phase phosphatidylethanolamine complex [68].

2.4.2.2. Clinical significance Galli *et al.* presented eight studies with multivariate analyses: two of those indicated that anti-PT were independent risk factors for thrombosis and three other similar studies showed that anti-PT added to the risk borne by LA or aCL. In this widespread analysis report, 37% of anti-PT and thrombosis associations were significant: only 3 out of 11 associations were significantly correlated to arterial thrombosis and 7 out of 18 with venous thrombosis. In conclusion, no clear association with thrombosis was found for anti-PT, irrespective of isotype, site, and type of event [59].

2.4.3. Annexin A5

ANXA5 is an anionic phospholipid-binding protein with an apparent molecular weight of 36 kDa. Based on its activity to interact specifically with acidic phospholipids, ANXA5 is used widely as a reagent to detect PS on the surface of apoptotic cells. As a radiolabeled probe, it is thus employed to detect apoptotic changes in cells or tissues of live animals. Its physiological roles in cells include inhibition of phospholipase A2, acting as a calcium ion channel, binding collagens and potent anti-coagulant activity by protecting vascular endothelium from aPL [69]. ANXA5 requires rather high calcium concentrations (in the 10-μM range) for phospholipid binding [70]. Regardless of the site of action, that is, the cytoplasmic or exoplasmic leaflets of cell membranes, the mechanistic basis of ANXA5 activity is mostly linked to its ability to form two-dimensional crystals on planar lipid bilayers [71]. ANXA5 forms this antithrombotic shield around procoagulant anionic phospholipids, which blocks their participation in phospholipid-dependent coagulation reactions. Without the shield, there is a net increase in the quantity of anionic phospholipids on cell membranes that are available to accelerate coagulation reactions. The formation of this protective shield is Ca^{++} dependent. Calcium has also been shown to promote the binding of ANXA5 to wells coated with a mixture of phospholipids including PS or PC. It was found that PS promoted binding of ANXA5 to the wells in presence of Ca^{++} [72]. It has been recently demonstrated that such a crystalline protein network on cell membranes opens a new portal for entry into the cell [73]. This network, specific for ANXA5, elicits budding, endocytotic vesicle formation, and cytoskeleton-dependent trafficking of the endocytotic vesicle. The novel, ANXA5-mediated internalization is independent of membrane ruffling and actin polymerization and can mediate the uptake of tissue factor in a macrophage cell model [74]. Downregulation of tissue factor through extracellular ANXA5 has also been observed in a mouse carotid artery injury model (same study). Such regulation of extracellular tissue factor levels through ANXA5-mediated cell entry might be part of a more general mechanism to control cell surface receptors under physiological stress conditions [71].

2.4.3.1. Antibody characterization IgG fractions from APS patients reduce the levels of ANXA5 on cultured trophoblasts and endothelial cells, and accelerate coagulation of plasma exposed to these cells [69]. The IgG fractions also reduce

the level of ANXA5 bound to noncellular phospholipid bilayers and this reduction depends on the presence of β2GPI and results in acceleration of coagulation. The hypothesis stating that disruption of the two-dimensional ANXA5 shield by aPL (with cofactor β2GPI) enabling the coagulation factors to bind and activate prothrombotic pathways has been shown by tissue immunohistochemistry, cell culture studies, coagulation assays with noncellular phospholipids, and competition experiments on artificial phospholipid bilayers [69]. Specifically, the single and combined effects of antibodies against ANXA5 (anti-ANXA5) and anti-β2GPI antibodies on binding of ANXA5 to negatively charged phosholipid membranes were examined on giant vesicles and were found to differentially effect the binding. The results indicate competition between ANXA5 and complexes of β2GPI-anti-β2GPI for the same binding sites and support the shield disruption hypothesis on procoagulant membranes [75].

2.4.3.2. Clinical significance Clinical studies have primarily focused on two groups of patients: having either pregnancy complications or systemic autoimmune diseases (including rheumatoid arthritis), with or without thrombotic events. The majority of studies indicate anti-ANXA5 as a strong risk factor for fetal loss. Anti-ANXA5 have been detected in some systemic autoimmune diseases, particularly in SLE with thrombotic events, and APS. However, there are some reports of the presence of anti-ANXA5 in patients with arterial thrombosis lacking criteria for APS or evident autoimmune disease (reviewed in [76]). ANXA5 is abundant in late stage atherosclerotic lesions and may play a role in cardiovascular disease. Sera from SLE patients with a history of cardiovascular disease inhibited ANXA5 binding to endothelium caused by IgG antibodies [77].

3. Cellular Microexovesicles (Microparticles) in Thrombosis and Hemostasis with Special Emphasis on APS

MVs can be defined as 0.1–1 μm cell-derived vesicular structures that are shed off cells into the circulation and therefore represent an important system of transport of matter and information within the body [8–11]. It was found that MVs can be released from cells (with failure of membrane asymmetry) that have been exposed to a procoagulative and/or inflammatory environment [78]. They can be released by all cell types upon activation or apoptosis [78]; moreover, they were suggested to play a role in vascular disease [79], inflammation [80], and communication of tumor cells with macrophages [81]. Generally, MVs are enriched in various bioactive molecules and may directly stimulate the release of pro- as well as anti-inflammatory mediators, transfer membrane receptors (such as chemokine receptors), proteins, mRNA and organelles (e.g., mitochondria) between cells, promote leukocyte rolling, deliver infectious agents into cells (for instance, human immunodeficiency virus, prions) [11], and induce immune cell apoptosis. Figure 1 shows an example of an erythrocyte membrane bud and a MV from the same sample.

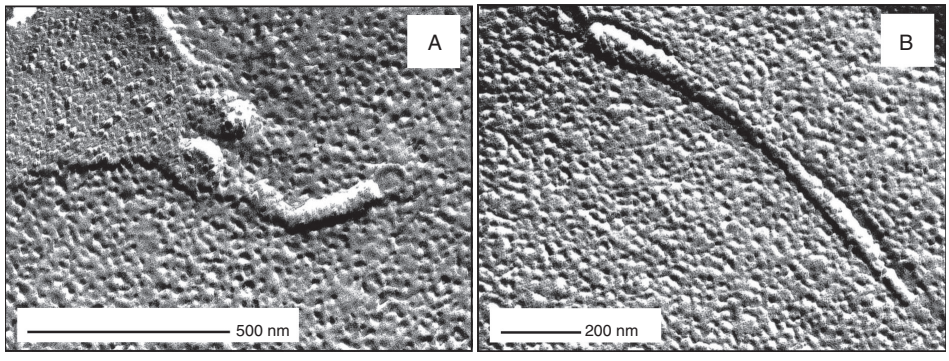

Figure 1 **Transmission electron microscopy micrographs of freeze–fracture replicas showing the tubular bud on top of the echinocyte spicule (A) and the free tubular microvesicle (MV) released from the membrane (B). The budding/vesiculation was induced by adding 40 μM of dodecyl-maltoside to the erythrocyte suspension. Adapted from [82].**

MVs are also a potential diagnostic tool as the analysis of their abundance and composition can convey information on processes that are taking place in a particular organism. The abundance of MVs can be measured by flow cytometry while staining by different cell surface markers can point to their possible origin and give information on processes in mother cells. For example, MVs contain varying amounts of surface-exposed PS which can be detected by ANXA5.

The function of MVs vary according to cellular origins and inducers of vesiculation. Hence, MVs can be pro-coagulant or anti-coagulant, but when the balance is disrupted in favor of the former population, this reflects an increased thrombotic risk. It was found that patients with APS have an increased level of MVs in blood [12].

Pinching off a MV from the cell membrane (called microvesiculation) is the final event in a complex process of membrane budding, a process which may be induced by various mechanisms reflected in changes of the local membrane curvature. These changes are strongly coupled to the lateral composition of the membrane which is—in turn—determined by the intrinsic properties of the molecules that constitute the structural domains, and nonlocal effects deriving from maximization of entropy, constraints upon the membrane area and enclosed volume, and interaction of each membrane leaflet with the surrounding solution. While the interdependence between the intrinsic shape of the molecules that constitute the membrane and the local membrane shape is an obvious feature in budding, also the above-mentioned nonlocal effects are important, especially in the initial phases, since they may drive the membrane to a point where the budding would more likely take place [83–87].

3.1. Mechanisms Leading to Microvesiculation

3.1.1. Initiation of the budding process by intercalation of the exogeneous molecules into the outer layer of the membrane

Within the bilayer couple hypothesis [88–90], the two membrane leaflets are strongly coupled due to the hydrophobic effect; therefore, changes in the difference between the areas of the two membrane leaflets may bend the membrane inward or

outward, (depending on the relative change of the two areas) thereby initiating the process of budding. If the area of the outer leaflet increased with respect to the area of the inner leaflet, the membrane would bend outward while if the area of the inner leaflet increased with respect to the area of the outer leaflet, the membrane would bend inward. Additionally, if the intrinsic shape of the part of the molecule intercalated into the membrane leaflet, it would also contribute to the change of the local membrane curvature [91]. The relative change in the leaflet areas can thus be induced by intercalating of exogeneous molecules into one of the leaflets. In early experiments, it was shown that the normal discoid shape of erythrocytes changed into echinocyte shape by addition of substances to the suspension which intercalated preferentially into the outer membrane leaflet [88]. Theoretical studies have shown that the parameter that drives the outward or inward folding of the membrane is indeed the difference between the outer and the inner membrane leaflet areas [92]. A method has been developed to calculate the equilibrium shape of the membrane by minimization of the membrane bending energy considering the membrane as a thin isotropic elastic shell [91, 93],

$$W_{\mathrm{b}} = \frac{k_{\mathrm{c}}}{2}\int_A (2H)^2 \mathrm{d}A, \tag{1}$$

where k_{c} is the membrane bending constant, $H = (C_1 + C_2)/2$ is the local mean curvature, C_1 and C_2 are the two principal membrane curvatures, $\mathrm{d}A$ is the area element, and A is the membrane area. The relevant geometrical constraints requiring fixed membrane area A

$$\int_A \mathrm{d}A = A \tag{2}$$

and fixed difference between the two membrane leaflet areas ΔA [92]

$$\delta\int_A 2H\mathrm{d}A = \Delta A, \tag{3}$$

where ΔA is the prescribed area difference and δ is the distance between the two neutral areas of the two membrane leaflets, are taken into account. The above variational problem can be expressed by a system of Euler–Lagrange differential equations which are solved numerically.

Figure 2 shows the calculated shapes of a confined membrane segment with prescribed area A and increasing difference between the two membrane leaflet areas ΔA which may develop by continuous intercalation of molecules into the outer membrane layer.

As the process of the budding proceeds, redistribution of membrane proteins as well as changes in cytoskeleton attachment occur; therefore, the composition of the MV that is eventually pinched off the membrane is a reflection of the sorting of membrane constituents that took place prior to the detachment of the MV from the membrane.

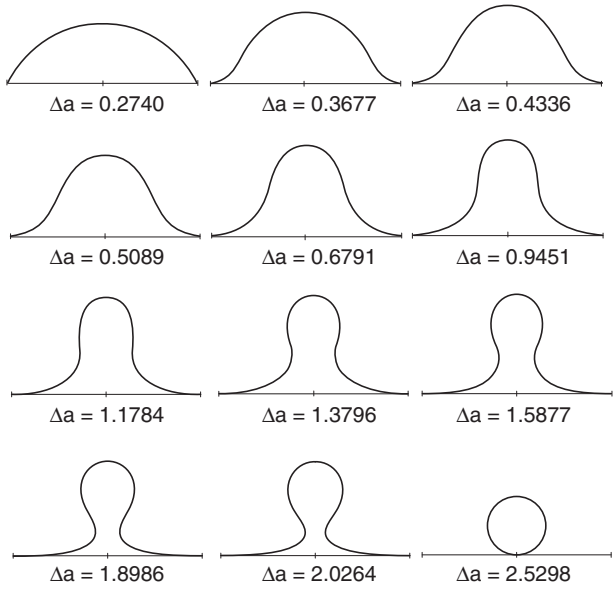

Figure 2 Calculated shapes of a confined membrane segment for increasing normalized difference between the two membrane leaflet areas $\Delta a = \Delta A/\pi\delta R_s$, where $R_s = \sqrt{A/\pi}$. The shapes correspond to the respective minima of the membrane bending energy at prescribed area of the segment A and prescribed normalized difference between the areas of the two membrane leaflets ΔA. Adapted from [85].

The membrane constituents are more or less free to move laterally over the membrane surface, so they would accumulate in regions of local curvature which are favorable for them—that is, which enable them to be in their lowest possible energetical state, while regions of unfavorable curvature would be depleted of these constituents. The direct interactions between the membrane constituents may promote separation of membrane constituents to form membrane rafts—mobile sphingolipid and cholesterol-based microdomains in the membrane. Rafts vary in composition and size (6–50 nm in diameter) [94–97], host-specific proteins, and can coalesce into larger, functional domains [98, 99]. The local clustering of raft elements, with a preference for high spherical curvature, and the concomitant local shape changes may be strongly coupled to form a part of the driving mechanism of the vesicle budding [100].

3.1.2. Curvature sorting of membrane constituents

Membrane constituents may be single molecules or small complexes of molecules (membrane nanodomains) (Fig. 3).

We assume that the membrane constituent of the i-th species as a result of its structure and local interactions energetically prefers a local geometry that is described by the two intrinsic principal curvatures ($C_{1m,i}$ and $C_{2m,i}$). If $C_{1m,i} = C_{2m,i}$, the in-plane orientation (Fig. 4) of the constituent is immaterial. Such a constituent is called isotropic (Fig. 3B). If $C_{1m,i} \neq C_{2m,i}$, the constituent is called anisotropic

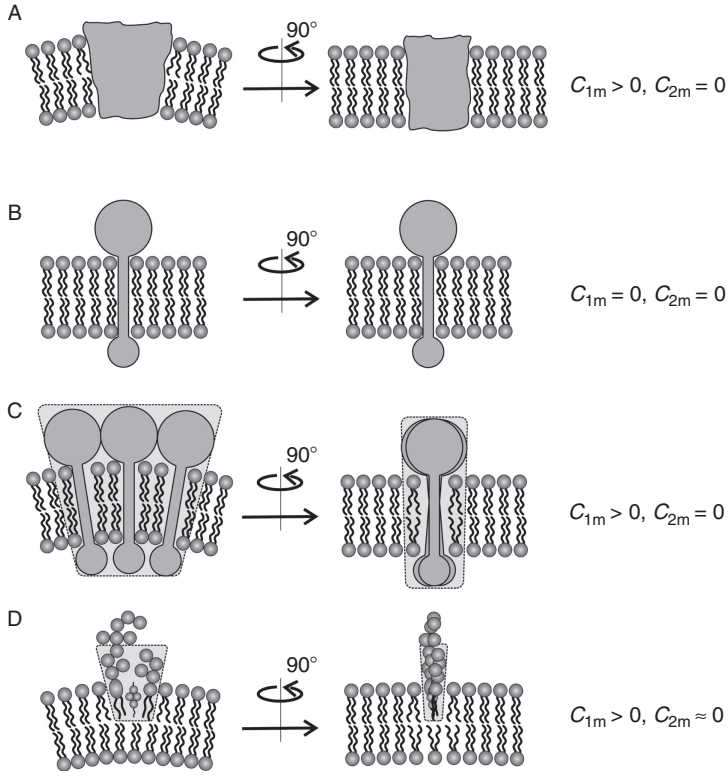

Figure 3 Schematic presentation of different membrane constituents. The constituents may be single molecules (A, B) and complexes of molecules (C) intercalated into both membrane leaflets (A–C) or into one leaflet only (D). The constituent (B) is isotropic, others are anisotropic.

(Fig. 3A,C,D). The orientation of anisotropic membrane constituent with respect to the local coordinate system of the membrane is important for its energy (Fig. 4). It is assumed that anisotropic constituent will on the average spend more time in the orientation that is energetically more favorable than in any other orientation.

The intrinsic principal curvatures of molecules are in general different ($C_{1m,i} \neq C_{2m,i}$) (Fig. 3). Also, small complexes of molecules that form a membrane constituent may have in general different intrinsic curvatures $C_{1m,i}$ and $C_{2m,i}$ from the intrinsic curvatures of the molecules which compose the constituent (Fig. 3).

The free energy of a single membrane constituent of the i-th kind can be written in the form [101]:

$$F_i = \frac{\xi_i}{2}(H - H_{m,i})^2 + \frac{\xi_i + \xi_i^*}{4}(D^2 + D_{m,i}^2) - kT \ln\left(I_o\left(\frac{(\xi_i + \xi_i^*)D_{m,i}D}{2kT}\right)\right), \tag{4}$$

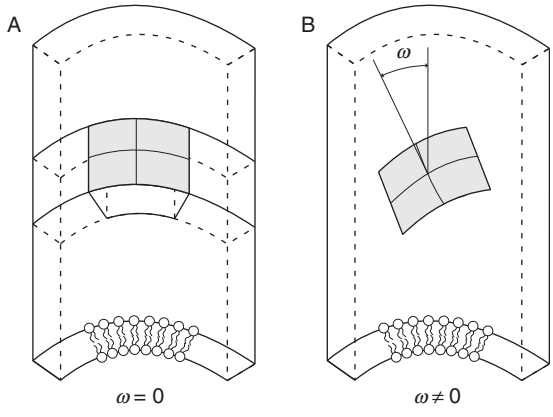

Figure 4 Schematic presentation of an anisotropic membrane constituent. The intrinsic principal directions are rotated for an angle ω with respect to the local principal directions of the membrane.

where ξ_i and ξ_i^* are the interaction constants, $H = (C_1 + C_2)/2$ and $D = |C_1 - C_2|/2 = \sqrt{H^2 - C_1 C_2}$ are the mean curvature and curvature deviator, and $H_{m,i}$ and $D_{m,i}$ are the intrinsic mean curvature and intrinsic curvature deviator describing the intrinsic shape of the membrane constituent of the i-th species, kT is the thermal energy, and I_0 is the modified Bessel function.

Assume a single (sufficiently large) membrane patch of lateral area A and local mean and deviatoric curvatures H and D, respectively. Let the membrane contain three constituent species, N_1 constituents of type $i = 1$, N_2 constituents of type $i = 2$, and N_3 constituents of type $i = 3$. All three molecular species can in general be anisotropic (by having a nonzero curvature deviator $D_{m,i}$). From the conservation of the overall number of constituents in the lipid layer (N), we express the number of molecules of first type N_1 as $N_1 = N - N_2 - N_3$. For the sake of simplicity, we assume that all three species occupy the same lateral cross-sectional area per constituent in the membrane layer $a = A/N$. The nature of the lipid bilayer allows its constituents to laterally redistribute. That is, in a nonhomogeneously curved lipid layer, the molecules of all species are assumed to migrate toward their energetically preferred membrane regions so as to minimize the overall free energy. We describe this degree of freedom by the local compositions of the species, namely m_2,m_3, and $m_1 = 1 - m_2 - m_3$, where $m_i = N_i/N$, are equal to the local fractions of the membrane area covered by the molecules of type 1, 2, and 3, respectively. We denote the average compositions $\bar{m}_i$ as:

$$\bar{m}_i = \frac{1}{A}\int_A m_i \mathrm{d}A. \tag{5}$$

The free energy per molecule $\bar{F}$ of the membrane layer includes the contribution of the constituents' ($f_i = F_i/kT$), the contribution of the configurational entropies

[101, 102], and the contribution of the direct interactions between molecules of the second type ($i = 2$), considered within the Bragg–Williams approximation [103],

$$\frac{\bar{F}}{kT} = \frac{N}{A}\int_A \left\{ \sum_{i=1}^{3} \left(m_i f_i + kT \left(m_i \ln \frac{m_i}{\bar{m}_i} - m_i + \bar{m}_i \right) \right) + \frac{wz_2}{2} m_2^2 \right\} \mathrm{d}A \quad (6)$$

where w is the constant of direct interactions between constituents of type $i = 2$ (in units of kT), and z_2 is the corresponding coordination number. We can construct a Lagrangian of the form:

$$L = \sum_{i=1}^{3} \left(m_i f_i + kT \left(m_i \ln \frac{m_i}{\bar{m}_i} - (m_i - \bar{m}_i) \right) + \tilde{\lambda}_i (m_i - \bar{m}_i) \right) + \frac{wz_2}{2} m_2^2 \quad (7)$$

where $\tilde{\lambda}_i$ are the Lagrangian multipliers. Inserting into the Lagrangian the relations $m_1 = 1 - m_2 - m_3$ and $\bar{m}_1 = 1 - \bar{m}_2 - \bar{m}_3$, we can eliminate one of the Lagrangian multipliers by defining $\lambda_2 = \tilde{\lambda}_2 - \tilde{\lambda}_1$ and $\lambda_3 = \tilde{\lambda}_3 - \tilde{\lambda}_1$. Using the Euler–Lagrange equations $\partial L/\partial m_2 = 0$ and $\partial L/\partial m_3 = 0$, we can derive an expression for composition m_3 in the form:

$$m_3 = \bar{m}_3 \frac{m_2 \mathrm{e}^{f_2 - f_3 + wz_2 m_2}}{1/A \int m_2 \mathrm{e}^{f_2 - f_3 + wz_2 m_2} \mathrm{d}A}, \quad (8)$$

while m_1 can be obtained from $m_1 = 1 - m_2 - m_3$. The equation for m_2 is in general an integral equation. However, for small direct interactions ($w \ll 1$), we can apply the expansion up to the first relevant term in w,

$$m_2 = m_2^0 (1 - wz_2 m_2^0 (1 - m_2^0)) \quad (9)$$

where

$$m_2^0 = \frac{\bar{m}_2 \mathrm{e}^{-f_2 - \lambda_2}}{\bar{m}_2 \mathrm{e}^{-f_2 - \lambda_2} + \bar{m}_3 \mathrm{e}^{-f_3 - \lambda_3} + \bar{m}_1 \mathrm{e}^{-f_1}} \quad (10)$$

is the value of m_2 for $w = 0$. The values of the Lagrangian multipliers λ_2 and λ_3 are obtained from the constraint (4,5).

For illustration, a case is considered where the membrane is assumed to be composed of lipid molecules (type $i = 1$) which for the sake of simplicity are taken to be isotropic (i.e., $D_{m,1} = 0$)), anisotropic constituents ($i = 2$) ($D_{m,2} \neq 0$), and isotropic conical constituents with a preference for a high spherical curvature ($i = 3$) ($D_{m,3} = 0$, $H_{m,3} \neq 0$). The constituents of type 2 and 3 are taken to be distributed only in the outer layer of the membrane bilayer. The closed membrane shape given in Fig. 5 was calculated by minimization of the Helfrich bending energy [Eq. (1)] as

explained elsewhere [104]. It was considered that while affecting the energy of the vesicle shape, the presence of the anisotropic constituents in the membrane does not substantially affect the shape itself [104].

It can be seen in Fig. 5 that the anisotropic saddle-like membrane constituents (m_2) are predominantly distributed in the region of the membrane neck, while the isotropic constituents with a preference for a highly isotropically curved membrane (m_3) are predominantly accumulated on the spherical daughter vesicle/bud. Increase of m_2 with increasing interaction constant w (not shown) indicates that the direct interactions between the constituents may play an important role in the energetics of the budding process and clustering of membrane constituents (i.e., raft formation).

It can be concluded that the budding process is promoted by the accumulation of anisotropic membrane constituents in the membrane necks and by accumulation of isotropic constituents that energetically prefer large positive curvature on the bud.

Below we present experimental evidence on the curvature sorting of membrane constituents.

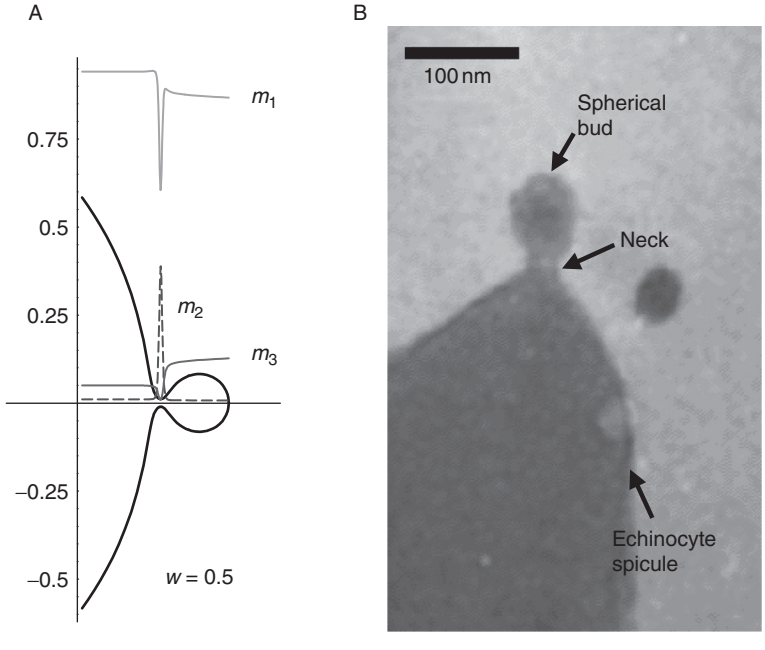

Figure 5 (A) Equilibrium lateral distribution of membrane constituents in the budding region of the bilayer membrane for a 3-component membrane (lipids: 1; anisotropic constituents: 2; isotropic conical constituents: 3). The axisymmetric closed membrane shape has a relative average mean curvature of 1.075 and a relative volume 0.99. The values are calculated relative to the sphere with radius $R_s = \sqrt{A/4\pi}$. The values of the model parameters are: $\xi_1 = 16$ kT nm^2, $H_{m,1} = D_{m,1} = 0$; $\xi_2 = 320$ kT nm^2, $H_{m,2} = 0$, $D_{m,2} = 0.3$ nm^{-1}, $m_2 = 0.01$, $z_2 = 6$; $\xi_3 = 240$ kT nm^2, $H_{m,3} = 0.3$ nm^{-1}, $D_{m,3} = 0$, $\bar{m}_3 = 0.05$; $\xi_i^* = 0$. (B) Spherical bud on the tip of the echinocyte spicule. Budding was induced by adding 40 μM of dodecylzwittergent to the suspension of erythrocytes. Adapted from [108] and [103].

Methods have been developed to induce budding, microexovesiculation, and endovesiculation of the erythrocyte membrane, for example, by exogeneously adding amphiphilic molecules to the erythrocyte suspension [105] or increasing cytosolic calcium level and to analyze the composition of the MVs [106]. It was found that composition of some membrane constituents in the MVs differs from the composition of the mother membrane and that the membrane cytoskeleton detaches prior to microexovesiculation [107].

Recently, the distribution of raft markers in curved membrane exvaginations and invaginations, induced in human erythrocytes by amphiphile treatment or increased cytosolic calcium level, was studied by fluorescence microscopy; cholera toxin subunit B and antibodies were used to detect raft components [100]. Figure 6A shows the exvaginated shape of erythrocytes treated with ionophore A23187 plus calcium. The spiculae are distributed around the spheroid main body of the cell. Membrane buds, apparently in the process of being released, can be seen on the tips of spiculae. A marked enrichment of stomatin, sorcin, and synexin was detected in calcium-induced erythrocyte spiculae (Fig. 6B1, C1, and D1). Clustering of rafts and membrane proteins in highly curved membrane regions (invaginations) and MVs has also been observed previously [107, 109].

In order to study the differential segregation of membrane proteins during budding by a complementary method, we isolated MVs shed by the erythrocytes upon the respective treatments and compared the relative amounts of several membrane marker proteins. As most of the MVs probably originate from the tips

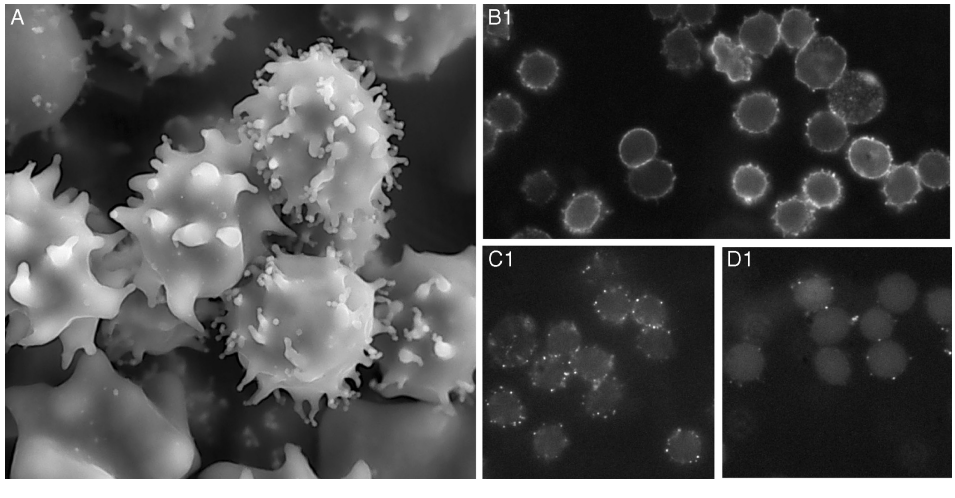

Figure 6 (A) Scanning electron micrograph showing exvaginated human erythrocytes following incubation with ionophore A23187 (1 mM, 10 min, 37 °C) in the presence of 3.8 mM calcium. (B1) Immunocytochemical detection of stomatin in erythrocytes treated with A23187 plus calcium. (C1) Immunocytochemical detection of sorcin in erythrocytes treated with A23187 plus calcium. (D1) Immunocytochemical detection of synexin in erythrocytes treated with A23187 plus calcium. Notably, the magnification is larger in A than in other micrographs. Adapted from [100].

of membrane protrusions [82], the membrane protein content of the released vesicle reflects the local membrane protein composition of the protrusions' tips. In accordance with previous results [107, 110, 111], the glycosylphosphatidylinositol-anchored acetylcholinesterase, which is a raft marker located at the exoplasmic side of the membrane, is found to be highly enriched in all types of highly curved MVs. The vesicular aliquots were normalized to acetylcholinesterase activity to show the differences in the depletion of the respective proteins relative to this raft marker. The MVs are strongly depleted in the peripheral membrane protein band 6 and the membrane skeletal components spectrin, band 4.1, band 4.2, and actin. Band 3 and the major integral raft components, stomatin and flotillin-2, are present in the MVs.

It was indicated that two complementary mechanisms may take place in the budding of heterogeneous membranes containing isotropic and anisotropic constituents: accumulation of saddle-preferring membrane constituents in the neck connecting the bud and the parent membrane [103] and accumulation of strongly spherically curved membrane-preferring constituents in the spherical region of the daughter vesicle/bud [100, 112–114]. On the basis of theoretical and experimental studies, it was concluded that membrane skeleton-detached, laterally mobile raft elements may sort into curved or flat membrane regions, dependent on their intrinsic molecular shape and/or direct interactions between the raft elements. Curvature sorting of membrane constituents explains enrichment or depletion of buds and MVs with respect to certain membrane constituents and/or membrane rafts.

3.2. Effect of β2GPI and aPL on Budding of Phospholipid Vesicles

In previous studies [115–117], giant phospholipid vesicles (GPVs) have been proven to be useful systems for determination of the effects of β2GPI and aPL on phospholipid membranes. Interest in these models was recently renewed due to their diagnostic and prognostic clinical potential. Below we present the results of our observations.

3.2.1. Methodology

β2GPI was purified from pooled human sera by affinity column chromatography. The monoclonal anti-β2GPI Cof-22 (generously provided by Prof. Takao Koike) obtained from BALB/c mice immunized with human β2GPI and recognizing domain III of β2GPI was used in a concentration of 1 μg/mL. IgG fractions were isolated from the sera of one patient with APS and from two children with atopic dermatitis containing high titers of IgG anti-β2GPI.

Monoclonal HCAL anti-β2GPI antibodies (chimeric mouse monoclonal antibodies containing the human Fc region), obtained from BALB/c mice immunized with human β2GPI [118] and recognizing domain V of β2GPI, were dialyzed in PBS. In all experiments, the final concentration of HCAL anti-β2GPI was 1 mg/l.

GPVs were prepared at room temperature (23 °C) by the electroformation method [119] with small modifications as described in detail in [120, 121]. Briefly, 10 μl of lipid mixture was applied to platinum electrodes. The solvent was allowed

to evaporate in a low vacuum for 2 h. The coated electrodes were placed in the electroformation chamber which was then filled with 0.2 M sucrose solution. An AC electric current with an amplitude of 5 V and a frequency of 10 Hz was applied to the electrodes for 2 h, which was followed by 2.5 V and 5 Hz for 15 min, 2.5 V and 2.5 Hz for 15 min, and finally 1 V and 1 Hz for 15 min. The content was rinsed out of the electroformation chamber with 0.2 M glucose solution and stored in a plastic test tube. Before placing the vesicles into the observation chamber, the sample was gently mixed. Unilamellar GPVs were prepared out of 10 mol% 1-pamitoyl-2-oleoyl-phosphatidylserine (POPS) and 90 mol% 1-pamitoyl-2-oleoyl-phosphatidylcholine (POPC). An individual GPV of medium size (diameter ~40–60 μm) and without visible irregularities on the surface was aspirated by a glass micropipette from the compartment containing GPVs, and then transferred to the compartment containing β2GPI (100 μg/ml) and/or anti-β2GPI or purified normal human IgG in the control experiments.

3.2.2. Experimental results

The budding of GVPs was observed for the period of 1 h in solution containing β2GPI (Fig. 7). Budding and release of daughter vesicles from GPV were demonstrated following transfer of GPV into the compartment containing β2GPI and Cof-22 (Fig. 8).

The effects were similar, but less pronounced, when using an IgG fraction from an APS patient. There were no changes observed using GPV and Cof-22 without β2GPI. When children's (atopic dermatitis) or normal human serum were used, no changes on the GPV were found.

The results of this study imply that β2GPI alone and in combination with anti-β2GPI promote the budding of phospholipid membrane. The budding of GPVs could be initiated by the insertion of the C-terminal loop of β2GPI into the outer layer of a phospholipid membrane. As the C-terminal loop of β2GPI is relatively short, it does not expand through the whole width of the outer layer of the membrane. Therefore, the insertion of the C-terminal loop in an external portion of the outer layer of the membrane causes an increase of the area of the outer layer of the phospholipid bilayer with respect to the area of the inner layer as well as an increase of the local curvature of the membrane. Consequently, the membrane is bent outward and curvature sorting of membrane constituents further promotes the formation of the bud and the neck.

The permeabilization and consequent fading of GPVs were observed, mostly in more spherical GPVs [120]. The volume of these GPVs was very close to the maximal volume that could be reached with a finite membrane area. Theoretically, as the mean shape of a vesicle approaches a sphere, the thermal shape fluctuations become smaller, since, for a sphere as a stationary shape, there is no space available for fluctuations at the constant volume. In the case of a nearly spherical vesicle, when additional molecules of β2GPI were inserted into the outer monolayer, the relative difference in the surface between the monolayers caused an increased tension in the inner monolayer, which could trigger a transient pore formation and consequent leaking of the membrane [122].

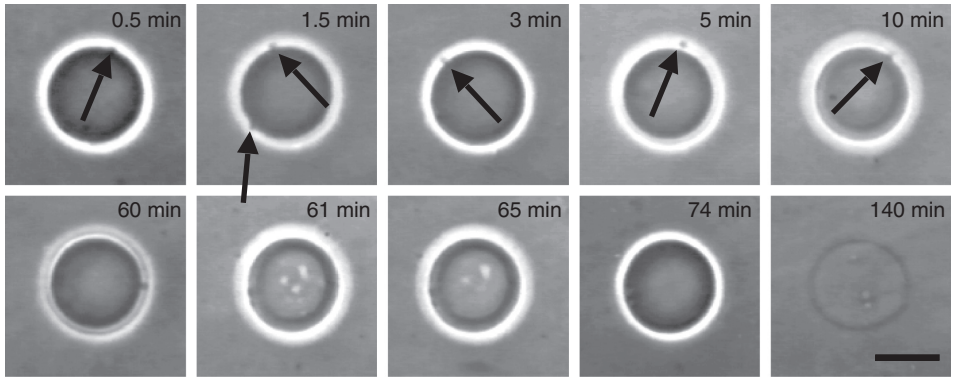

Figure 7 Budding of GPVs in solution containing 100 mg/ml of β2GPI. Two buds (marked by black arrows) were formed on the GPV about 90 s after transfer of the GPV into the solution containing β2GPI. No significant changes were seen during further observation for up to 60 min. Only one bud is visible 5 min after transfer as the other one was out of focus. Bar = 20 μm. Adapted from [120].

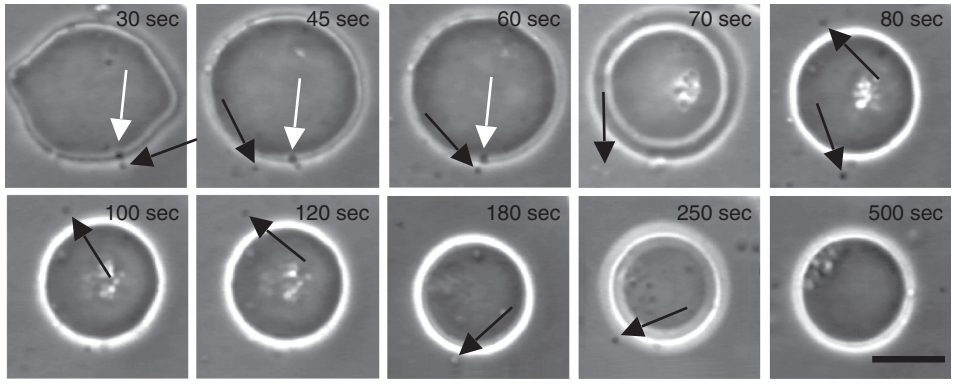

Figure 8 Budding of GPVs transferred into solution containing 100 mg/ml β2GPI and Cof-22. Intense budding of the GPV started quickly after the transfer. Small daughter vesicles (marked with black arrow) separated and moved away from the GPV. Steady state of the GPV was reached after ~3 min. Bar = 20 μm. Adapted from [120].

4. Coalescence of Membranes Caused by β2GPI and aPL

Collective interactions between membraneous structures are of great interest, especially as they can be mediated by protein cofactors and aPL involved in APS. Close approach and coalescence of membranes enable the onset of biochemical processes involving molecules of interacting membranes. Below we give experimental evidence on the effect of β2GPI and aPL on the coalescence of GPVs and suggest a possible mechanism for explanation of the mediating effect of the aPL.

4.1. Experimental Evidence on the Effect of β2GPI and aPL on Coalescence of Phospholipid Vesicles

4.1.1. Methodology

β2GPI (Hyphen BioMed, France) was resuspended, aliquoted, and stored at -70 °C. In all experiments, the final concentration of β2GPI in PBS was 100 mg/l, which is approximately half the concentration of physiological β2GPI in normal human plasma (about 200 mg/l) [123, 124]. An IgG fraction was isolated from the serum of a patient with APS. The IgG fraction contained high titers of anti-β2GPI as determined by affinity purification on a 2-ml protein-G column (Pierce, Rockford, USA), using the protocol recommended by the manufacturer. The IgG fraction was equilibrated against PBS (pH 7.4) in a desalting column. This IgG fraction gave comparable results to whole serum in an anti-β2GPI ELISA performed as described previously [125]. The levels of anti-β2GPI in the IgG preparations were considered as medium range, amounting to about a half of the anti-β2GPI levels in serum.

The synthetic lipids CL (1,1′2,2′-tetraoleoyl cardiolipin), POPC (1-palmitoyl-2-oleoyl-*sn*-glycero-3-phosphocholine), and cholesterol were purchased from Avanti Polar Lipids, Inc.

Appropriate volumes of POPC, CL, and cholesterol, all dissolved in a 2:1 chloroform/methanol mixture, were combined in a glass jar and thoroughly mixed. For charged CL vesicles, POPC, cholesterol, and CL were mixed in the proportion of 2:2:1. For neutral POPC GPVs, POPC and cholesterol were mixed in the proportion of 4:1. Cholesterol was added to POPC to increase the longevity of GPVs. The GPVs were left for sedimentation under gravity for one day at 4 °C. 200–400 μl of the sediment was collected from the bottom of the tube and used for a series of experiments. GPVs were observed by a Zeiss Axiovert 200 inverted microscope with phase contrast optics (objective magnification 100×) and recorded by a Sony XC-77CE video camera. The solution containing GPVs was placed in an observation chamber made from cover glasses sealed with grease. The larger (bottom) cover glass was covered by two smaller (18 × 18 mm glasses), each having a small semicircular part removed at one side. Covering the bottom glass with two opposing smaller glasses thus formed a circular opening in the middle of the observation chamber. The circular opening enabled subsequent addition of PBS-dissolved protein. In all experiments, the solution of GPVs (45 μl) was placed in the observation chamber. The solution containing the substance under investigation (5 μl) was added through the circular opening in the middle of the observation chamber. The osmolarity of the sample containing GPVs was 205 mosm/l (measured by a Knauf Semiosmometer). The observation chamber was mounted on a temperature-regulated microscope stage. In observing the coalescence of the population of GPVs, the temperature was kept at 40 °C while the budding of the GPVs was induced by increasing the temperature above the room temperature [126].

4.1.2. Experimental results

The solution of GPVs contained a heterogeneous population of shapes. Most of the GPVs were flaccid. Thermal fluctuations of shapes were notable. Few minutes after the addition of the solution containing dissolved β2GPI, thermal fluctuations of

GPVs diminished, protrusions disintegrated into spherical fragments while GPVs attained nearly spherical shapes. This phase of the morphological changes was observed also after addition of PBS alone. With PBS, the sample ultimately contained nearly spherical fluctuating GPVs. With β2GPI however, nearly spherical fragments joined into two or multi-compartment structures composed of spherical parts and flat walls (Fig. 9A and B). Furthermore, GPVs adhered to the bottom of the glass slide and ceased to fluctuate. Large surfaces of contact between spherical compartments could be observed. The sample ultimately contained motionless aggregates of GPVs which adhered to the bottom of the glass slide. GPVs in the sample retained their shape until the end of observation (one hour).

When the IgG fraction of a patient with APS was added to the solution with GPVs, a similar time course was observed as when β2GPI was added to GPVs (Fig. 9C and D). However, in addition to the suppression of fluctuations and adhesion of vesicles, we observed lateral segregation within the membrane in the time scale of minutes (Fig. 9F). In the next step, we added β2GPI to the solution of GPVs one hour following addition of the patients' IgG fraction. We have observed additional transformations of GPVs into ghosts and also sudden bursts of some GPVs. The sample was eventually formed from adhered GPVs and ghosts, bi- and multi-compartment GPV and ghost formations, some exhibiting lateral segregation and regions of larger curvature (Fig. 9E). The reversed order of addition of β2GPI and the patients' IgG fraction in the same time intervals resulted in similar observations; however, we did not directly observe bursts of the membrane.

4.2. Theoretical Description of the Coalescence of Membranes: Interaction Between Charged Surfaces Mediated by Ions with Dimeric Distribution of Charge

The interaction between like-charged membranes is described theoretically by two interacting electric double layers consisting of two charged flat surfaces, each of the area A, separated by a distance D (Fig. 10). It is assumed that each surface bears uniformly distributed charge with surface charge density $\sigma_0 \leq 0$ describing negative charge of CL headgroups. The space between the charged surfaces is filled with an electrolyte solution, one of the ion species representing antibodies. The antibodies are composed of four chains, two heavy ones and two light ones, organized into a dimeric structure. In this work, for simplicity, it is assumed that an antibody molecule is a globular multivalent ion with a simple distribution of charge where two equal effective charges e are separated by a distance l (Fig. 10). The antibodies are taken to be equal and indistinguishable.

The ions in the solution distribute according to the electrostatic and entropic effects. Because of the electrostatic effects, it could be expected that counterions are attracted by the charged surfaces while coions are repelled by these surfaces so that the electric field is shielded by the distribution of ions. In equilibrium, an equilibrium configuration is attained which yields consistently related distribution functions of ions, electric field, and free energy of the system. The dependence of the free energy on the distance between the surfaces gives the interaction between the surfaces. If the free energy decreases with increasing distance, the interaction is

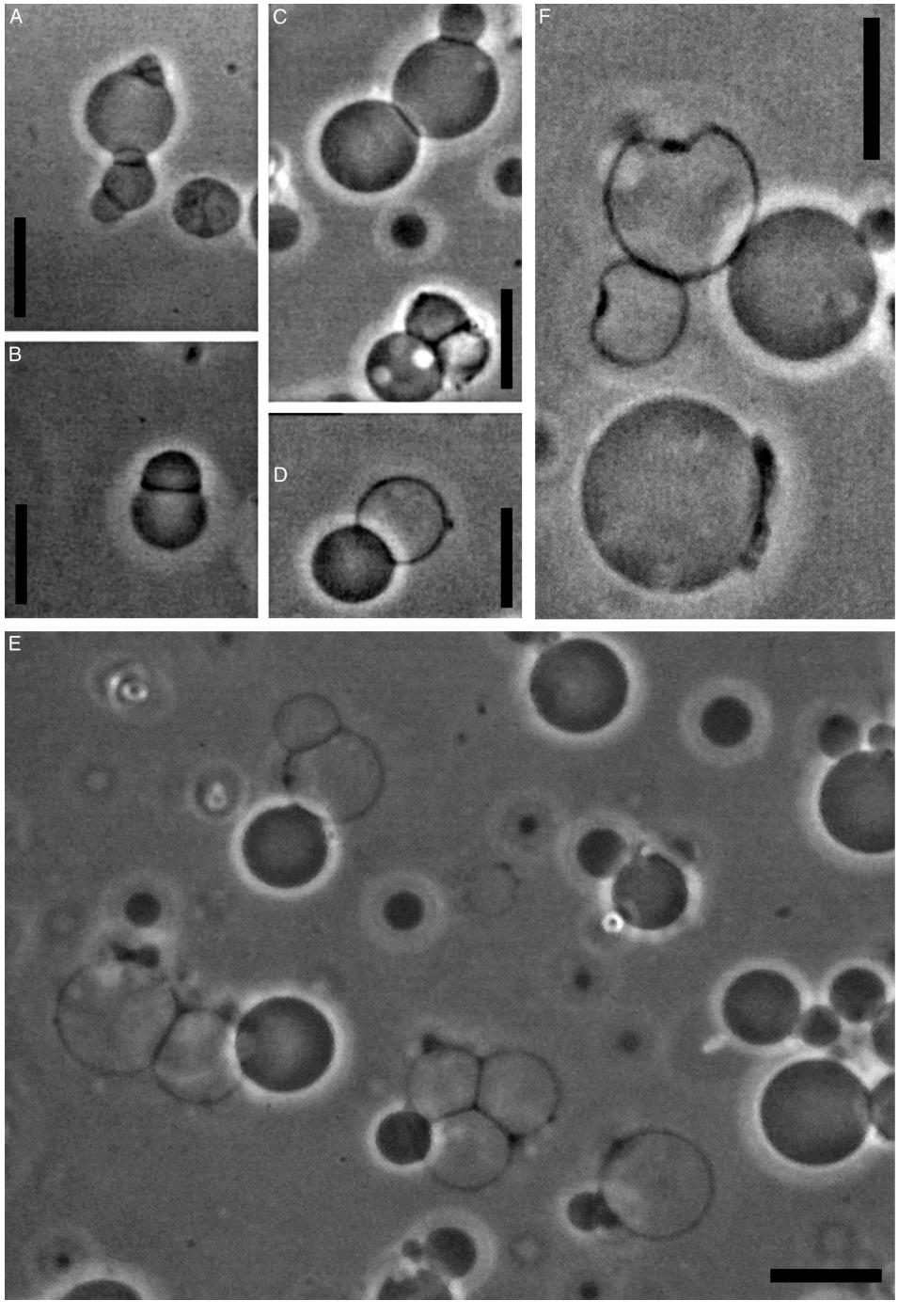

Figure 9 Effect of β2GPI and IgG fraction of a patient with APS syndrome on GPVs containing cardiolipin (CL) and cholesterol; sticky formations induced by addition of β2GPI (A and C) and by addition of IgG fraction of a patient with APS (B and D). A flat wall dividing the vesicular compartments (area of contact of the two vesicles) is indicated as the two solutions are of different

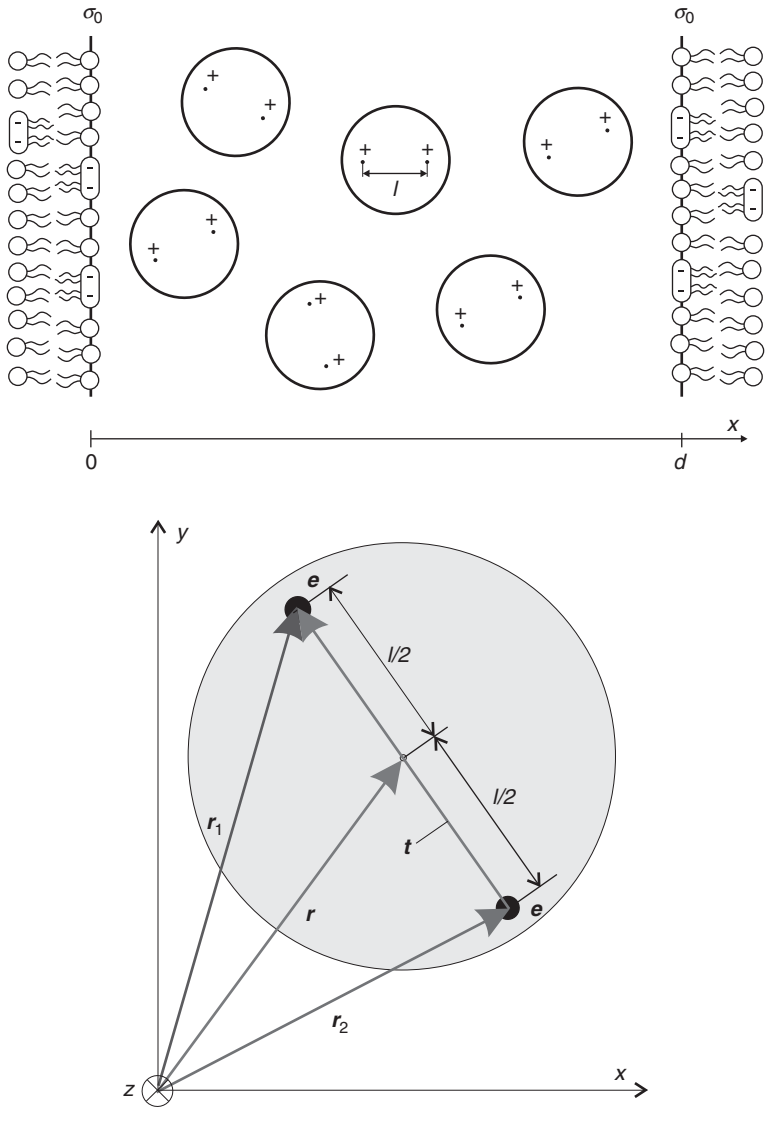

Figure 10 Schematic illustration of two like-charged flat surfaces with surface charge density σ_0 and area A, separated by a distance d (upper). The space between the surfaces is filled with electrolyte solution. The globular ions with internal distribution of charge represent the antibodies with dimeric structure. Within an antibody, the charge distribution is represented by two point charges separated by a distance l (lower).

contents (D). The areas of contact seem larger after addition of β2GPI (A and C). Regions of the lateral separation can be observed after the addition of IgG fraction of a patient with APS (B and D). CL-containing GPVs after addition of IgG fraction of a patient with APS (E). Lateral separation within the membrane is indicated (darker regions within the membrane). Some GPVs transformed into ghosts (light vesicles) indicating formation of membrane pores. The sample with CL-containing GPVs (F). Bars denote 10 μm. Adapted from [127].

repulsive while it is attractive if the free energy increases with increasing distance. If the global minimum of the equilibrium free energy with respect to the distance between the charged surfaces exists, the system attains the stable shape at the corresponding distance between the surfaces.

Here, we focus on the role of the spatial distribution of charge within ions. We consider the simplest case of a symmetric electrolyte, where the antibodies have the role of counterions. As the assumed distribution of charge is not spherically symmetric, different orientations of the ion with respect to the electric field are not energetically equivalent. It can be expected that the ion will spend on the average more time in the orientation that is energetically more favorable. The orientation represents an additional degree of freedom within the system that could at certain conditions in the system give rise to an attractive interaction between the like-charged membranes. Below we present the theory taking into account these effects and show that orientational effects of the particular spatial distribution of charges within ions for certain model parameters cause an attractive interaction between membranes.

4.2.1. Electric field created by a single species of dimeric ions and a charged surface

When the internal distribution of charge within the ion is taken into account, the microscopic density of charge is not uniform so that the macroscopic and the microscopic densities are in general different.

The center of the mass of the dimeric ion is given by the radius vector $\mathbf{r}$. The two charges are then located at $\mathbf{r}_1 = \mathbf{r} + (l/2)\mathbf{t}$ and $\mathbf{r}_2 = \mathbf{r} - (l/2)\mathbf{t}$ where $\mathbf{t} = (\sin\theta\cos\phi, \sin\theta\sin\phi, \cos\theta)$ is the director defining the orientation of the dimeric ion (Fig. 10). The microscopic density of charge is given by [128]:

$$\eta(\mathbf{r}') = e\delta(\mathbf{r}' - \mathbf{r}_1) + e\delta(\mathbf{r}' - \mathbf{r}_2), \tag{11}$$

where $\delta(\mathbf{r})$ is the Dirac delta function. At a given distribution of ions, the average microscopic density of charge of a chosen ion $\langle\eta\rangle$ is obtained by [128]:

$$\langle\eta\rangle = \int \mathrm{d}^3\mathbf{r}' m(\mathbf{r}')\eta(\mathbf{r}') = em(\mathbf{r}_1) + em(\mathbf{r}_2), \tag{12}$$

where m is the number of ions per volume and $\langle\ldots\rangle$ stands for spatial averaging.

For small enough distances between the charges within the ion l, the functions $m(\mathbf{r}_1)$ and $m(\mathbf{r}_2)$ can be expanded into Taylor series up to the terms of the second order with respect to the distance l,

$$m\left(\mathbf{r} \pm \frac{l}{2}\mathbf{t}\right) = m(\mathbf{r}) \pm \frac{l}{2}\sum_i \mathrm{t}_i \frac{\partial m(\mathbf{r})}{\partial \mathrm{r}_i} + \frac{l^2}{8}\sum_{ij} t_i t_j \frac{\partial^2 m(\mathbf{r})}{\partial r_i \partial r_j}, \tag{13}$$

where $t_i (i = x,y,z)$ are the components of the vector $\mathbf{t}$. The expansions (13) are inserted into Eq. (12) to yield:

$$\langle \eta \rangle = 2em + \frac{el^2}{4} \sum_{ij} t_i t_j \frac{\partial^2 m(\mathbf{r})}{\partial r_i \partial r_j}, \tag{14}$$

where the first term in the above equation ($2em$) corresponds to the macroscopic density of charge ρ while the second term represents the quadrupolar contribution to $\langle \eta \rangle$. The linear terms representing the density of the dipoles cancel out.

The tensor $\underline{T} = t_i t_j$ can be written in the matrix form [129]:

$$\underline{T} = \begin{pmatrix} \sin^2\theta \cos^2\phi & \sin^2\theta \sin\phi \cos\phi & \sin\theta \cos\theta \cos\phi \\ \sin^2\theta \cos\phi \sin\phi & \sin^2\theta \sin^2\phi & \sin\theta \cos\theta \sin\phi \\ \sin\theta \cos\theta \cos\phi & \sin\theta \cos\theta \sin\phi & \cos^2\theta \end{pmatrix} \tag{15}$$

In flat electric double layer, the density of charge varies only in the direction perpendicular to the charged surfaces x, therefore $m(\mathbf{r}) \equiv m(x)$, so that

$$\langle \eta \rangle = 2em + \frac{el^2}{4} \Delta m(x) \cos^2\theta \tag{16}$$

where $\Delta m(x) = \mathrm{d}^2 m / \mathrm{d}x^2$.

In calculating an effective density of charge ρ_{eff}, all possible orientations of a dimeric ion are taken into account,

$$\rho_{\text{eff}} = \frac{1}{4\pi} \int_0^{2\pi} \mathrm{d}\phi \int_0^{\pi} \langle \eta \rangle \sin\theta \, \mathrm{d}\theta, \tag{17}$$

where $\mathrm{d}\boldsymbol{\Omega} = \sin\theta \, \mathrm{d}\theta \, \mathrm{d}\phi$. Performing the necessary integrations yields [130]

$$\rho_{\text{eff}} = 2em + \frac{el^2 \Delta m}{12} \tag{18}$$

The effective density of charge ρ_{eff} enters the basic law of the electromagnetism expressed by the Maxwell equation [128]

$$\varepsilon \varepsilon_0 \nabla \cdot \mathbf{E} = \rho_{\text{eff}}, \tag{19}$$

where ε is the permittivity of the solution and ε_0 is the permittivity of the free space. Inserting Eq. (18) into the above Maxwell equation yields:

$$\varepsilon \varepsilon_0 \nabla \cdot \mathbf{E} = 2em + \frac{el^2}{12} \Delta m \tag{20}$$

while considering that $\mathbf{E} = -\nabla\Phi$ we obtain the Poisson equation

$$\varepsilon\varepsilon_0\Delta\Phi = -\rho_{\text{eff}}. \tag{21}$$

Eq. (20) is rewritten into

$$\nabla \cdot \left(\varepsilon\varepsilon_0\mathbf{E} - \frac{el^2}{12}\nabla m\right) = 2em, \tag{22}$$

wherefrom we can deduce the electric field density $\mathbf{D}$,

$$\mathbf{D} = \varepsilon\varepsilon_0\mathbf{E} - \frac{el^2}{12}\nabla m \tag{23}$$

The boundary condition is stated by considering that the normal component of the density of the electric field is connected to the surface density of charge

$$\mathbf{D} \cdot \mathbf{n} = \sigma_0, \tag{24}$$

where $\mathbf{n}$ is the vector in the direction of the surface normal and σ_0 is the area density of charge at the charged surface. It was taken that there is no electric field outside the electrolyte solution. This can be justified by low dielectric constant of the phospholipid tails. It follows from Eqs. (23) and (24) and from the definition of the derivative with respect to the direction of the normal to the surface $E_n = -\partial\Phi/\partial n$ that [130]

$$\varepsilon\varepsilon_0\frac{\partial\Phi}{\partial n} = -\sigma_{\text{eff}}, \tag{25}$$

where

$$\sigma_{\text{eff}} = \sigma_0 + \frac{el^2}{12}\frac{\partial m}{\partial n} \tag{26}$$

is the effective area density of charge at the charged surface.

4.2.2. Electrostatic energy of the electric double layer composed of a charged surface and electrolyte solution containing dimeric counterions and coions

We consider a charged surface with area density of charge σ_0 in contact with electrolyte solution containing dimeric counterions and coions. To make the derivation more simple, we include in the model also dimeric coions which turn

out to be strongly depleted from the system for relevant surface densities of charge but affect the results only negligibly [130]. The local concentrations of counterions and coions are denoted by m_+ and m_-, respectively. Because of the spatial separation of the charges along the dimeric ion, the effective volume charge density ρ_{eff}, receives contributions from the local concentrations of both species and also from their second derivatives representing the internal quadrupolar distribution of charge within an individual ion [Eq. (18)] [130],

$$\rho_{\text{eff}} = 2e(m_+ - m_-) + \frac{el^2}{12}(\Delta m_+ - \Delta m_-) \tag{27}$$

Similarly, the effective area density of charge at the charged surface is subject both to the charges on the surface and to the gradient of the concentrations,

$$\sigma_{\text{eff}} = \sigma_0 + \frac{el^2}{12}\left[\left(\frac{\partial m_+}{\partial n}\right)_A - \left(\frac{\partial m_-}{\partial n}\right)_A\right]. \tag{28}$$

The electrostatic free energy can be written as [128]:

$$F_{\text{el}} = \frac{\varepsilon\varepsilon_0}{2}\int_V (\nabla\Phi)^2 \mathrm{d}V = \frac{1}{2}\int_V \Phi\rho_{\text{eff}}\mathrm{d}V + \frac{1}{2}\int_A \Phi_A\sigma_{\text{eff}}\mathrm{d}A, \tag{29}$$

where $\mathrm{d}V$ is the volume element, $\mathrm{d}A$ is the area element, and Φ_A is the potential at the charged surface. Using the expressions for the effective densities of charge [Eqs. (27) and (28)] and Green's theorem, we reexpress F_{el} as:

$$F_{\text{el}} = \frac{1}{2}\int_V (m_+ - m_-)\left[2e\Phi + \frac{el^2}{12}\Delta\Phi\right]\mathrm{d}V + \frac{1}{2}\int_A \left[\sigma_0\Phi_A + \frac{el^2}{12}(m_+ - m_-)\frac{\partial\Phi}{\partial n}\right] \tag{30}$$

To derive the differential equation for the electric potential, we consider in the free energy also the contribution of the distributional entropy of ions F_{entr}. In the entropy, ions of the same species are taken to be dimensionless, equal, and indistinguishable. Thus, the free energy of the system F is:

$$F = F_{\text{el}} + F_{\text{entr}} \tag{31}$$

where [131]

$$F_{\text{entr}} = \int_V \left[m_+ \ln \frac{m_+}{m_0} + n_- \ln \frac{m_-}{m_0} - (m_+ + m_- - 2m_0)\right]\mathrm{d}V \tag{32}$$

where m_0 denotes the bulk concentration of the dimeric ions. We chose the reference state where $F(m_+ \equiv m_- \equiv m_0) = 0$.

In thermal equilibrium, the free energy F must be minimal with respect to the distributions of ions m_+ and m_-. To find the corresponding equilibrium distributions, we perform the first variation of $F(m_+, m_-)$, resulting in

$$\delta F = \frac{el^2}{12}\int_A \left(\frac{\partial\Phi}{\partial n}\right)_A (\delta m_+ - \delta m_-)\mathrm{d}A + \int_V \delta m_+ \left[2e\Phi + \frac{el^2}{12}\Delta\Phi + \ln\frac{m_+}{m_0}\right]\mathrm{d}V + \int_V \delta m_- \left[-2e\Phi - \frac{el^2}{12}\Delta\Phi + \ln\frac{m_-}{m_0}\right]\mathrm{d}V \tag{33}$$

Vanishing of δF for arbitrary δm_- and δm_+ gives rise to both the Boltzmann distributions [130]:

$$m_\pm = m_0 \exp\left[\mp\left(2e\Phi + \frac{el^2}{12}\Delta\Phi\right)\right] \tag{34}$$

and the boundary condition at the charged surfaces

$$\left(\frac{\partial\Phi}{\partial n}\right)_A = 0 \tag{35}$$

Note that Eq. (35) implies $\sigma_{\mathrm{eff}} = 0$, indicating the tendency of the dimeric ions to fully neutralize the bare charges on the charged surfaces. Complete neutralization can occur only for $l > 0$ without a prohibitively large entropic penalty of immobilizing the ions onto the charged surfaces.

Inserting $m_\pm$ from Eq. (34) into the Poisson equation yields the differential equation which we express in terms of the dimensionless electrostatic potential $\Psi = 2e\Phi/kT$. In the following we shall also use dimensionless spatial coordinates, $\bar{x} = x/l_D$ and so on, scaled by the Debye length $l_D = 1/\kappa$ with $\kappa^2 = 4 \times 8\pi l_B \mathrm{lm}_0$ where $l_B = e^2/4\pi\varepsilon\varepsilon_0 = 0.7$ nm is the Bjerrum length in water. We then obtain a fourth order, nonlinear, partial differential equation [130]

$$\Delta\Psi = \sinh(\Psi + \xi^2\Delta\Psi) + \xi^2\Delta\sinh(\Psi + \xi^2\Delta\Psi) \tag{36}$$

The above equation depends on the dimensionless parameter:

$$\xi = \frac{\kappa l}{\sqrt{24}} \tag{37}$$

that expresses the effective distance between the charges within the dimeric ion (Fig. 10). For $\xi = 0$, the differential equation reduces to $\Delta\Psi = \sinh \Psi$ which is the familiar equation used for a symmetric salt solution of structureless, point-like ions.

Solving the differential equation [Eq. (36)] requires the specification of two boundary conditions at the charged surfaces. The first one is given by $(\partial\Psi/\partial n)_A = 0$; see Eq. (35). To formulate the second boundary condition, it is convenient to express the (local) surface charge density of the charged surfaces, $\sigma_0 = pe/8\pi l_B l_D$, in terms of the dimensionless charge density, $p = \pm 8\pi l_B l_D/a$, where a is the (local) area per surface charge (the sign of the charged surface is determined by the sign of p). The second boundary condition $\sigma_{\text{eff}} = 0$, can be written as [130]:

$$\frac{p}{\xi^4} = \cosh(\Psi + \xi^2 \Delta\Psi) \frac{\partial}{\partial n} \Delta\Psi \tag{38}$$

Upon insertion of the equilibrium distribution for $m_\pm$ into F, we can show that the free energy can be calculated by the charging process [132]:

$$F = \int_A \mathrm{d}a \int_0^{\sigma_0} \Phi(\sigma_0') \, \mathrm{d}\sigma_0' = \frac{1}{16\pi l_B l_D} \int_A \mathrm{d}a \int_0^p \Psi(p') \mathrm{d}p' \tag{39}$$

4.2.3. The Debye–Hückel limit

In the Debye–Hückel (DH) regime, the electrostatic potential is small everywhere ($\Psi \ll 1$) and linearization of the differential equation [Eq. (36)] yields

$$\xi^4 \nabla^4 \Psi + (2\xi^2 - 1)\Delta\Psi + \Psi = 0 \tag{40}$$

where ∇^4 is the biharmonic operator. The boundary condition, Eq. (38) yields [130] $p/\xi^4 = \partial(\Delta\Psi)/\partial n$.

Consider two large, like-charged, planar surfaces, located at (dimensionless) positions $\bar{x} = 0$ and $\bar{x} = \bar{d} = d/l_D$, each having area $A/2$ and bare surface charge density σ_0 (with corresponding scaled surface charge density p). The electrostatic potential depends only on the $\bar{x}$-direction, and we must solve the equation $\xi^4 \Psi'''' + (2\xi^2 - 1)\Psi'' + \Psi = 0$ with the boundary conditions $\Psi'(0) = \Psi'(\bar{d}) = 0$ and $\Psi'''(0) = -\Psi'''(\bar{d}) = p/\xi^4$. The solution can be written as $\Psi(\bar{x}) = \sum_{i=1}^4 B_i e^{-\omega_i \bar{x}}$ with $\omega_3 = -\omega_1$, $\omega_4 = -\omega_2$, and [130]

$$B_i = \frac{(-1)^i p}{\xi^4 \omega_i (\omega_1^2 - \omega_2^2)(1 - e^{-\bar{d}\omega_i})}, \qquad \omega_{1,2} = \frac{1 \pm \sqrt{1 - 4\xi^2}}{2\xi^2} \tag{41}$$

Most notably, for $\xi > 1/2$, the potential Ψ exhibits damped oscillations whereas for $\xi > 1/2$ it decays monotonically. For the potential at the surfaces, we find $\Psi(0) = \Psi(\bar{d}) = pC(\xi, \bar{d})$ where the function $C(\xi, \bar{d})$ is given by [130]:

$$C(\xi, \bar{d}) = \frac{1}{\xi^4(\omega_1^2 - \omega_2^2)} \left[\frac{1}{\omega_2} \coth\frac{\bar{d}\omega_2}{2} - \frac{1}{\omega_1} \coth\frac{\bar{d}\omega_1}{2} \right] \qquad (42)$$

Upon insertion of $\Psi(0)$ into Eq. (39), we obtain the free energy $F = pNC(\xi, \bar{d})/2$ where $N = (\sigma_0/e)(A/2)$ is the number of fixed charges on each of the two flat surfaces. The function $C(\xi, \bar{d})$ determines the nature of the interaction between the like-charged macroionic surfaces.

For two isolated surfaces ($d \to \infty$; the left diagram of Fig. 11 shows the potential for some selected cases), we obtain that $C(\xi, \bar{d} \to \infty) = 1$ and the surface potential $\Psi(0) = p$ as well as the free energy $F = pN/2$ are independent of ξ. In fact, this is the familiar Debye-Huckel result for point-like divalent salt ions [132].

The interaction between two like-charged planar surfaces represented by the normalized free energy $C = 2F/Np$ in dependence on their mutual distance d for $\xi = 0$, 0.5, and 0.7 is presented in Fig. 11 (right diagram). For $\xi < ½$, the interaction is always repulsive. For $\xi = 1/2$, we obtain $C(\xi = 1/2, \bar{d}) = \coth\bar{d} + \bar{d}/\sinh^2\bar{d}$ which still is a monotonously decaying function of $\bar{d}$, implying repulsion between the two surfaces. However, for $\xi > ½$, the interaction turns attractive above a sufficiently large separation $\bar{d} = \bar{d}^*$ between the two surfaces.

Figure 12 shows position $\bar{d}^*$ at which $C(\xi > 1/2, \bar{d}^*)$ adopts a minimum, in dependence on the parameter ξ expressing the effective separation between the two charges within the dimeric ion [Eq. (37)]. A border of the phase diagram is shown separating the repulsive from the attractive regime. For example, $\xi = 0.7$

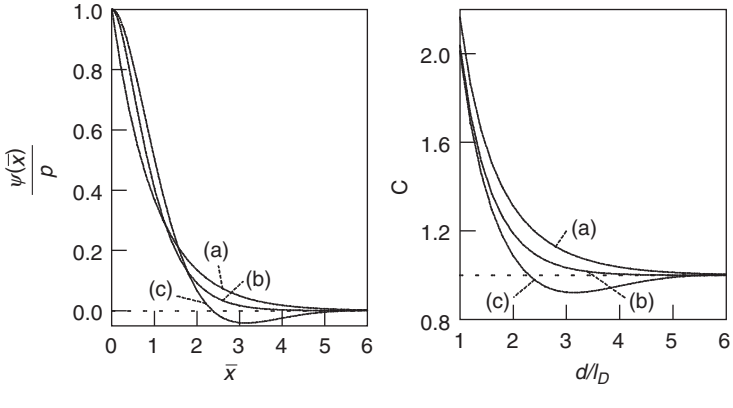

Figure 11 Results for the Debye-Huckel regime. Left diagram: The normalized potential, Ψ/p, of an isolated planar surface as a function of the scaled distance, $\bar{x} = x/l_D$ to that surface. Right diagram: The normalized free energy $C = 2F/Np$ as a function of the distance $\bar{d} = d/l_D$ between two charged surfaces. Both diagrams show the cases $\bar{x} = x/l_D$ for $\xi = 0$ (a), $\xi = 0.5$ (b), and $\xi = 0.7$ (c). Adapted from [130].

(corresponding to $l = 3.4l_D$) results in an energetic minimum at $\bar{d}^* = 3.2$ (corresponding to $d = 3.2l_D$). Hence, the dimeric ions just match the optimal separation between the charged surfaces, indicating that a bridging mechanism is responsible for the attractive interactions.

5. The Effects of ANXA5, β2GPI and aPL on Phospholipid Membranes

In order to study additional possible mechanisms preventing the exposure of procoagulant surfaces, GPVs with fluorescence-labeled ANXA5 were studied. As it was given in Section 2.4.3, ANXA5 is believed to form a protective shield by binding to negatively charged phospholipids thereby interfering with mechanisms involved in vascular thrombosis and pregnancy complications. The disruption of the ANXA5 shield by aPL [69] previously proposed the mechanism of pro-thrombotic action of aPL and indicated their possible involvement in fetal loss in APS. Antibodies in the presence of β2GPI compete with ANXA5 for the same binding sites on phospholipids causing the disruption of the protective ANXA5 shield on the procoagulant surfaces enhancing the activation of coagulation factors.

In order to study the influence of β2GPI on the binding of ANXA5 to the negatively charged phospholipids in the presence of anti-β2GPI and anti-ANXA5, the GPVs were prepared out of 15 mol% POPS and 85 mol% POPC as described in Section 3.2.1. Using fluorescent microscopy, the accumulation of ANXA5 conjugated with ALEXA-fluor 488 on the GPV surfaces in the presence of purified IgG containing anti-β2GPI or anti-ANXA5 (with addition of β2GPI and 3 mM $CaCl_2$) was measured. Purified IgG fractions were derived from four different

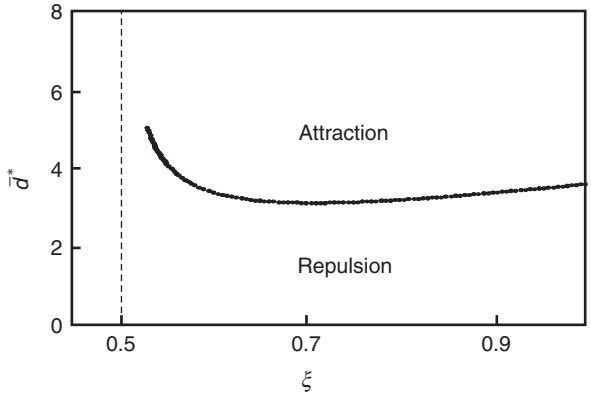

Figure 12 Results for the Debye-Huckel regime. The equilibrium distance between the charged surfaces $\bar{d}^*$ in dependence on the parameter ξ expressing the effective separation between the two charges within the dimeric ion κl. The repulsive and attractive regions are marked. Adapted from [130].

human sera (APS anti-β2GPI, systemic sclerosis anti-ANXA5, anti-ANXA5 blood donor, aPL negative control).

The ANXA5 fluorescent signal was stronger and its development was significantly faster in the presence of anti-ANXA5 sera as compared to the case when anti-β2GPI and control sera were present in the solution. A clear dependency of time and dose reduction of fluorescent ANXA5 emission on GPVs by anti-β2GPI is shown in Fig. 13.

A distinct difference in the influence of anti-β2GPI compared with anti-ANXA5 on the ANXA5 binding to the negatively charged phospholipids exists on GPVs, which could suggest different mechanisms of their pathogenic action: anti-β2GPI acting as a procoagulant and anti-ANXA5 interfering with ANXA5 binding.

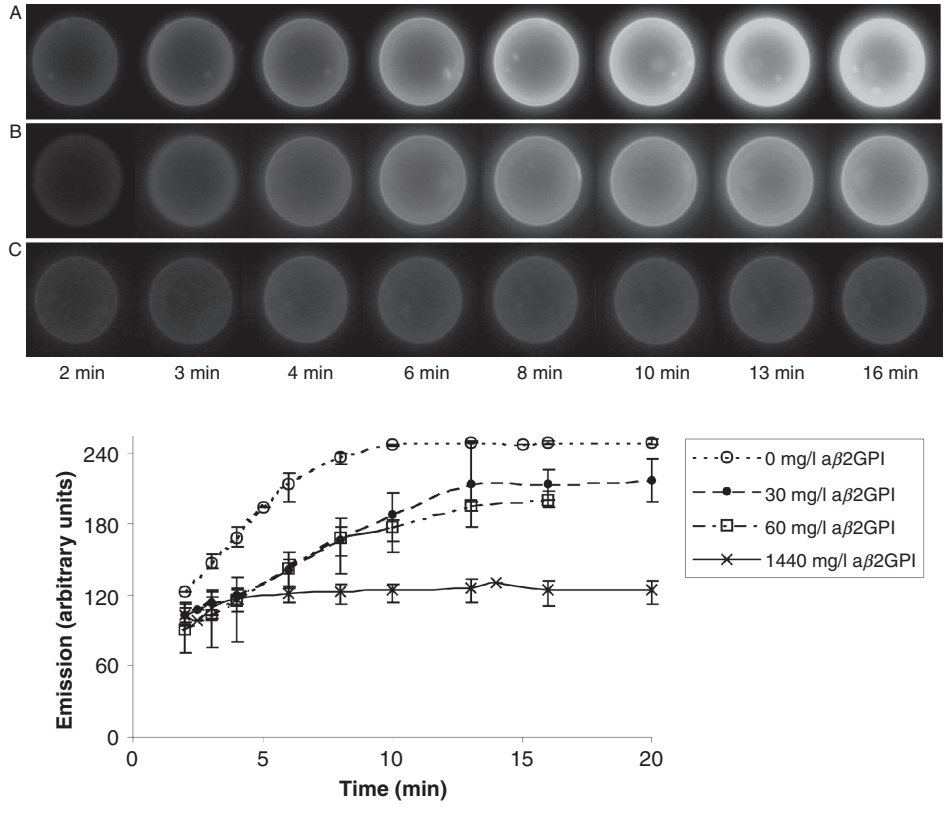

Figure 13 (Upper panel) Micrograph images of GPV transferred into the test solution containing fluorescent ANXA5, Ca^{++}, and β2GPI in the final concentration of 105 mg/l and (A) no anti-β2GPI; (B) 60 mg/l anti-β2GPI; and (C) 1440 mg/l anti-β2GPI. Time after the transfer is indicated below images. (Lower panel) The influence of anti-β2GPI at different concentrations on the binding of fluorescent ANXA5 in the presence of β2GPI (105 mg/l) and Ca^{++}. Each line represents the average growth of emission at a particular time for three GPVs; bars indicate the maximum and minimum values. a.u., arbitrary units). Reprinted from [75], with permission from Oxford University Press.

These results support the proposed destructive role of anti-β2GPI on the ANXA5-protective shield on the negatively charged phospholipids.

6. Conclusions

Studies of physical mechanisms involved in budding of cell membranes and interactions between membraneous structures can importantly contribute to the knowledge of the physiological roles of aPL antibodies and their protein cofactors involved in APS.

We have observed that β2GPI caused budding of PS-containing GPVs while the effect was enhanced when both β2GPI and Cof-22 antibodies were present in the solution. The Cof-22 antibodies alone had no effect, while the effect of the IgG fraction of the patient with APS was weak. β2GPI and the IgG fraction of the patient caused coalescence of the CL-containing GPVs. We observed permeabilization of the GPV membrane due to the presence of Cof-22 antibodies and IgG fraction of the patient with APS. It was shown that anti-ANXA5 and anti-β2GPI antibodies have different effects on the ANXA5 protective shield in GPVs.

The mechanisms involved in budding are based on the increase of the difference between the two membrane leaflet areas and on the curvature sorting of the membrane constituents. There seem to be multiple mechanisms underlying the coalescence of membranes. We have shown that orientational ordering of dimeric ions (representing the antibodies) can lead to an attractive interaction between the like-charged membranes—as observed in experiments.

GPVs and erythrocytes have proven to be a convenient system for the study of the effects of protein cofactors and aPL on the membraneous structures. In turn, experiments with plasma proteins have contributed to an advance in the electric double layer theory.

Orientational ordering of the molecules (both, in-plane ordering of membrane constituents as well as of ions with spatial distribution of charge in solution) represent a unifying mechanism underlying the budding process as well as the coalescence of membranes. The orientational ordering represents degrees of freedom within the system which can lower the free energy and promote different processes.

We hope that experiments and constructed theoretical models presented in this work will be followed by many studies that will reveal new and useful knowledge on the APS and related disorders.

ACKNOWLEDGMENTS

The authors are grateful to coauthors of the published works ([30, 58, 75, 76, 82, 85, 101–104, 108, 120, 121, 125, 127, 129–131]) for their collaboration. The work of S. Sodin-Šemrl was supported, during the writing of this chapter, by the MC-IRG #028414. The figures were reproduced with permission from the publishers.

REFERENCES

[1] G.R. Hughes, Thrombosis, abortion, cerebral disease, and the lupus anticoagulant, Br. Med. J. (Clin. Res. Ed.) 287 (1983) 1088–1089.
[2] M. Galli, D. Luciani, G. Bertolini, T. Barbui, Anti-beta 2-glycoprotein I, antiprothrombin antibodies, and the risk of thrombosis in the antiphospholipid syndrome, Blood 102 (2003) 2717–2723.
[3] E. Matsuura, Y. Igarashi, M. Fujimoto, K. Ichikawa, T. Koike, Anticardiolipin cofactor(s) and differential diagnosis of autoimmune disease, Lancet 336 (1990) 177–178.
[4] P. McNeil, R.J. Simpson, C.N. Chesterman, S.A. Krilis, Anti-phospholipid antibodies are directed against a complex antigen that includes a lipid-binding inhibitor of coagulation: β2-glycoprotein I (apolipoprotein H), Proc. Natl. Acad. Sci. USA 87 (1990) 4120–4124.
[5] P.G. de Groot, M. van Lummel, M. Pennings, R. Urbanus, H. Bas de Laat, P.J. Lenting, R.H. Derksen, Beta2-glycoprotein I and LDL-receptor family members, Thromb. Res. 114 (2004) 455–459.
[6] P.G. de Groot, R.H. Derksen, Pathophysiology of antiphospholipid antibodies, Neth. J. Med. 62 (2004) 267–272.
[7] W. Lim, M.A. Crowther, J.W. Eikelboom, Management of antiphospholipid antibody syndrome: a systematic review, JAMA 295 (2006) 1050–1057.
[8] T.J. Greenwalt, The how and why of exocytic vesicles, Transfusion 46 (2006) 143–152.
[9] D.D. Taylor, P.H. Black, Neoplastic and developmental importance of plasma membrane vesicles, Am. Zool. 26 (1987) 411–415.
[10] T.L. Whiteside, Tumour-derived exosomes or microvesicles: Another mechanism of tumour escape from the host immune system? Br. J. Cancer 92 (2005) 209–211.
[11] J. Ratajczak, M. Wysoczynski, F. Hayek, A. Janowska-Wieczorek, M.Z. Ratajczak, Membrane-derived microvesicles: important and underappreciated mediators of cell to cell communication, Leukemia 20 (2006) 1487–1495.
[12] F. Dignat-George, L. Camoin-Jau, F. Sabatier, D. Arnoux, F. Anfosso, N. Bardin, V. Veit, V. Combes, S. Gentile, V. Moal, M. Sanmarco, J. Sampol, Endothelial microparticles: A potential contribution to the thrombotic complications of the antiphospholipid syndrome, Thromb. Haemost. 91 (2004) 667–673.
[13] R.F. Zwaal, A.J. Schroit, Pathophysiologic implications of membrane phospholipid asymmetry in blood cells, Blood 89 (1997) 1121–1132.
[14] A. Zachowski, Phospholipids in animal eukaryotic membranes: transverse asymmetry and movement, Biochem. J. 294 (1993) 1–14.
[15] B. Perret, H.J. Chap, L. Douste-Blazy, Asymmetric distribution of arachidonic acid in the plasma membrane of human platelets. A determination using purified phospholipases and a rapid method for membrane isolation, Biochim. Biophys. Acta 556 (1979) 434–446.
[16] R.A. Schlegel, P. Williamson, Phosphatidylserine, a death knell, Cell Death Differ. 8 (2001) 551–563.
[17] V.A. Fadok, P.M. Henson, Apoptosis: giving phosphatidylserine recognition an assist-with a twist, Curr. Biol. 13 (2003) R655–R657.
[18] D. Dolis, C. Moreau, A. Zachowski, P.F. Devaux, Aminophospholipid translocase and proteins involved in transmembrane phospholipid traffic, Biophys. Chem. 68 (1997) 221–231.
[19] A. Zachowski, Phospholipids in animal eukaryotic membranes: Transverse asymmetry and movement, Biochem. J. 294 (1993) 1–14.
[20] M. Ikeda, A. Kihara, Y. Igarashi, Lipid asymmetry of the eukaryotic plasma membrane: Functions and related enzymes, Biol. Pharm. Bull. 29 (2006) 1542–1546.
[21] C. Alessandri, M. Sorice, M. Bombardieri, P. Conigliaro, A. Longo, T. Garofalo, V. Manganelli, F. Conti, M.D. Esposti, G. Valesini, Antiphospholipid reactivity against cardiolipin metabolites occurring during endothelial cell apoptosis, Arthritis Res. Ther. 8 (2006) R180–R191.
[22] S. Horkko, E. Miller, E. Dudl, P. Reaven, L.K. Curtiss, N.J. Zvaifler, R. Terkeltaub, S.S. Pierangeli, D.W. Branch, W. Palinski, J.L. Witztum, Antiphospholipid antibodies are

directed against epitopes of oxidized phospholipids. Recognition of cardiolipin by monoclonal antibodies to epitopes of oxidized low density lipoprotein, J. Clin. Invest. 98 (1996) 815–825.
[23] M. Sorice, A. Circella, R. Misasi, V. Pittoni, T. Garofalo, A. Cirelli, A. Pavan, G.M. Pontieri, G. Valesini, Cardiolipin on the surface of apoptotic cells as a possible trigger for antiphospholipids antibodies, Clin. Exp. Immunol. 122 (2000) 277–284.
[24] R. Subang, J.S. Levine, A.S. Janoff, S.M. Davidson, T.F. Taraschi, T. Koike, S.R. Minchey, M. Whiteside, M. Tannenbaum, J. Rauch, Phospholipid-bound beta 2-glycoprotein I induces the production of anti-phospholipid antibodies, J. Autoimmun. 15 (2000) 21–32.
[25] A. Tincani, G. Balestrieri, F. Allegri, M. Cinquini, M. Vianelli, M. Taglietti, M. Sanmarco, K. Ichikawa, T. Koike, P. Meroni, M.C. Boffa, Overview on anticardiolipin ELISA standardization, J. Autoimmun. 15 (2000) 195–197.
[26] E.M. Bevers, P. Comfurius, J.L. van Rijn, H.C. Hemker, R.F. Zwaal, Generation of prothrombin-converting activity and the exposure of phosphatidylserine at the outer surface of platelets, Eur. J. Biochem. 122 (1982) 429–436.
[27] E.M. Bevers, P. Comfurius, R.F. Zwaal, Changes in membrane phospholipid distribution during platelet activation, Biochim. Biophys. Acta 736 (1983) 57–66.
[28] P. Comfurius, P. Williamson, E.F. Smeets, R.A. Schlegel, E.M. Bevers, R.F. Zwaal, Reconstitution of phospholipid scramblase activity from human blood platelets, Biochemistry 35 (1996) 7631–7634.
[29] D. Smrz, L. Draberova, P. Draber, Non-apoptotic phosphatidylserine externalization induced by engagement of glycosylphosphatidylinositol-anchored proteins, J. Biol. Chem. 282 (2007) 10487–10497.
[30] B. Božič, T. Kveder, M. Stegnar, E. Morosini-Berus, M. Kos-Golja, P. Peternel, B. Rozman, Influence of degraded phosphatidylserine on binding of antiphospholipid antibodies, Int. Arch. Allergy Immunol. 112 (1997) 19–26.
[31] J.A. McIntyre, Antiphospholipid antibodies in implantation failures, Am. J. Reprod. Immunol. 49 (2003) 221–229.
[32] J. Lozier, N. Takahashi, F.W. Putnam, Complete amino acid sequence of human plasma beta 2-glycoprotein I, Proc. Natl. Acad. Sci. USA 81 (1984) 3640–3644.
[33] R. Schwarzenbacher, K. Zeth, K. Diederichs, A. Gries, G.M. Kostner, P. Laggner, R. Prassl, Crystal structure of human beta2-glycoprotein I: Implications for phospholipid binding and the antiphospholipid syndrome, EMBO J. 18 (1999) 6228–6239.
[34] J. Hunt, S. Krilis, The fifth domain of beta 2-glycoprotein I contains a phospholipid binding site (Cys281-Cys288) and a region recognized by anticardiolipin antibodies, J. Immunol. 152 (1994) 653–659.
[35] B. Bouma, P.G. de Groot, J.M. van den Elsen, R.B. Ravelli, A. Schouten, M.J. Simmelink, R.H. Derksen, J. Kroon, P. Gros, Adhesion mechanism of human beta(2)-glycoprotein I to phospholipids based on its crystal structure, EMBO J. 18 (1999) 5166–5174.
[36] A. Chonn, S.C. Semple, P.R. Cullis, Association of blood proteins with large unilamellar liposomes *in vivo*. Relation to circulation lifetimes, J. Biol. Chem. 267 (1992) 18759–18765.
[37] A. Gries, J. Nimpf, H. Wurm, G.M. Kostner, T. Kenner, Characterization of isoelectric subspecies of asialo-beta 2-glycoprotein I, Biochem. J. 260 (1989) 531–534.
[38] G.M. Willems, M.P. Janssen, M.M. Pelsers, P. Comfurius, M. Galli, R.F. Zwaal, E.M. Bevers, Role of divalency in the high-affinity binding of anticardiolipin antibody-beta 2-glycoprotein I complexes to lipid membranes, Biochemistry 35 (1996) 13833–13842.
[39] S. Sodin-Šemrl, B. Rozman, β-2-glycoprotein I and its clinical significance: From gene sequence to protein levels, Autoimmun. Rev. 6 (2007) 547–552.
[40] H. Wurm, E. Beubler, E. Polz, A. Holasek, G. Kostner, Studies on the possible function of beta 2-glycoprotein-I: influence in the triglyceride metabolism in the rat, Metabolism 31 (1982) 484–486.
[41] K. Kobayashi, M. Kishi, T. Atsumi, M.L. Bertolaccini, H. Makino, N. Sakairi, I. Yamamoto, T. Yasuda, M.A. Khamashta, G.R. Hughes, T. Koike, D.R. Voelker, E. Matsuura, Circulating oxidized LDL forms complexes with beta2-glycoprotein I: implication as an atherogenic autoantigen, J. Lipid Res. 44 (2003) 716–726.

[42] D. Harats, J. George, Beta2-glycoprotein I and atherosclerosis, Curr. Opin. Lipidol. 12 (2001) 543–546.
[43] J. George, N. Yacov, E. Breitbart, L. Bangio, A. Shaish, B. Gilburd, Y. Shoenfeld, D. Harats, Suppression of early atherosclerosis in LDL-receptor deficient mice by oral tolerance with beta 2-glycoprotein I, Cardiovasc. Res. 62 (2004) 603–609.
[44] I. Schousboe, Beta 2-glycoprotein I: A plasma inhibitor of the contact activation of the intrinsic blood coagulation pathway, Blood 66 (1985) 1086–1091.
[45] J. Nimpf, E.M. Bevers, P.H. Bomans, U. Till, H. Wurm, G.M. Kostner, R.F. Zwaal, Prothrombinase activity of human platelets is inhibited by beta 2-glycoprotein-I, Biochim. Biophys. Acta 884 (1986) 142–149.
[46] J. Nimpf, H. Wurm, G.M. Kostner, Beta 2-glycoprotein-I (apo-H) inhibits the release reaction of human platelets during ADP-induced aggregation, Atherosclerosis 63 (1987) 109–114.
[47] T. Mori, H. Takeya, J. Nishioka, E.C. Gabazza, K. Suzuki, Beta 2-glycoprotein I modulates the anticoagulant activity of activated protein C on the phospholipid surface, Thromb. Haemost. 75 (1996) 49–55.
[48] F. Conti, M. Sorice, A. Circella, C. Alessandri, V. Pittoni, B. Caronti, C. Calderaro, T. Griggi, R. Misasi, G. Valesini, Beta-2-glycoprotein I expression on monocytes is increased in anti-phospholipid antibody syndrome and correlates with tissue factor expression, Clin. Exp. Immunol. 132 (2003) 509–516.
[49] K. Ma, R. Simantov, J.C. Zhang, R. Silverstein, K.A. Hajjar, K.R. McCrae, High affinity binding of beta 2-glycoprotein I to human endothelial cells is mediated by annexin II, J. Biol. Chem. 275 (2000) 15541–15548.
[50] E. Raschi, C. Testoni, D. Bosisio, M.O. Borghi, T. Koike, A. Mantovani, P.L. Meroni, Role of the MyD88 transduction signaling pathway in endothelial activation by antiphospholipid antibodies, Blood 101 (2003) 3495–3500.
[51] S.K. Moestrup, I. Schousboe, C. Jacobsen, J.R. Leheste, E.I. Christensen, T.E. Willnow, Beta2-glycoprotein-I (apolipoprotein H) and beta2-glycoprotein-I-phospholipid complex harbor a recognition site for the endocytic receptor megalin, J. Clin. Invest. 102 (1998) 902–909.
[52] M. van Lummel, M.T. Pennings, R.H. Derksen, R.T. Urbanus, B.C. Lutters, N. Kaldenhoven, P.G. de Groot, The binding site in beta2-glycoprotein I for ApoER2′ on platelets is located in domain V, J. Biol. Chem. 280 (2005) 36729–36736.
[53] K. Balasubramanian, A.J. Schroit, Characterization of phosphatidylserine-dependent beta2-glycoprotein I macrophage interactions. Implications for apoptotic cell clearance by phagocytes, J. Biol. Chem. 273 (1998) 29272–29277.
[54] N. Del Papa, Y.H. Sheng, E. Raschi, D.A. Kandiah, A. Tincani, M.A. Khamashta, T. Atsumi, G.R. Hughes, K. Ichikawa, T. Koike, G. Balestrieri, S.A. Krilis, P.L. Meroni, Human beta 2-glycoprotein I binds to endothelial cells through a cluster of lysine residues that are critical for anionic phospholipid binding and offers epitopes for anti-beta 2-glycoprotein I antibodies, J. Immunol. 160 (1998) 5572–5578.
[55] M. Vega-Ostertag, K. Casper, R. Swerlick, D. Ferrara, E.N. Harris, S.S. Pierangeli, Involvement of p38 MAPK in the up-regulation of tissue factor on endothelial cells by antiphospholipid antibodies, Arthritis Rheum. 52 (2005) 1545–1554.
[56] T. Atsumi, O. Amengual, S. Yasuda, E. Matsuura, T. Koike, Research around beta2-glycoprotein I: A major target for antiphospholipid antibodies, Autoimmunity 38 (2005) 377–381.
[57] M. Merten, S. Motamedy, S. Ramamurthy, F.C. Arnett, P. Thiagarajan, Sulfatides: targets for anti-phospholipid antibodies, Circulation 108 (2003) 2082–2087.
[58] S. Čučnik, T. Kveder, B. Rozman, B. Božič, Binding of high-avidity anti-beta2-glycoprotein I antibodies, Rheumatology (Oxford) 43 (2004) 1353–1356.
[59] M. Galli, D. Luciani, G. Bertolini, T. Barbui, Lupus anticoagulants are stronger risk factors for thrombosis than anticardiolipin antibodies in the antiphospholipid syndrome: A systematic review of the literature, Blood 101 (2003) 1827–1832.
[60] G. Reber, P. de Moerloose, Anti-beta2-glycoprotein I antibodies—when and how should they be measured? Thromb Res. 114 (2004) 527–531.
[61] D. Faden, A. Tincani, P. Tanzi, L. Spatola, A. Lojacono, M. Tarantini, G. Balestrieri, Anti-beta 2 glycoprotein I antibodies in a general obstetric population: Peliminary results on the

prevalence and correlation with pregnancy outcome. Anti-beta2-glycoprotein I antibodies are associated with some obstetrical complications, mainly preeclampsia-eclampsia, Eur. J. Obstet. Gynecol. Reprod. Biol. 73 (1997) 37–42.
[62] R.M. Lee, W. Emlen, J.R. Scott, D.W. Branch, R.M. Silver, Anti-beta2-glycoprotein I antibodies in women with recurrent spontaneous abortion, unexplained fetal death, and antiphospholipid syndrome, Am. J. Obstet. Gynecol. 181 (1999) 642–648.
[63] S. Miyakis, M.D. Lockshin, T. Atsumi, D.W. Branch, R.L. Brey, R. Cervera, R.H. Derksen, P.G. DE Groot, T. Koike, P.L. Meroni, G. Reber, Y. Shoenfeld, A. Tincani, P.G. Vlachoyiannopoulos, S.A. Krilis, International consensus statement on an update of the classification criteria for definite antiphospholipid syndrome (APS), J. Thromb. Haemost. 4 (2006) 295–306.
[64] D.A. Lane, H. Philippou, J.A. Huntington, Directing thrombin, Blood 106 (2005) 2605–2612.
[65] E.W. Davie, J.D. Kulman, An overview of the structure and function of thrombin, Semin. Thromb. Hemost. 32 (2006) 3–15.
[66] J.A. Huntington, Molecular recognition mechanisms of thrombin, J. Thromb. Haemost. 3 (2005) 1861–1872.
[67] M. Galli, T. Barbui, Antiprothrombin antibodies: Detection and clinical significance in the antiphospholipid syndrome, Blood 93 (1999) 2149–2157.
[68] J. Rauch, M. Tannenbaum, A.S. Janoff, Distinguishing plasma lupus anticoagulants from anti-factor antibodies using hexagonal (II) phase phospholipids, Thromb. Haemost. 62 (1989) 892–896.
[69] J.H. Rand, X.X. Wu, H.A. Andree, J.B. Ross, E. Rusinova, M.G. Gascon-Lema, C. Calandri, P.C. Harpel, Antiphospholipid antibodies accelerate plasma coagulation by inhibiting annexin-V binding to phospholipids: A ''lupus procoagulant'' phenomenon, Blood 92 (1998) 1652–1660.
[70] P. Raynal, H.B. Pollard, Annexins: The problem of assessing the biological role for a gene family of multifunctional calcium- and phospholipid-binding proteins, Biochim. Biophys. Acta 1197 (1994) 63–93.
[71] A. Markoff, V. Gerke, Expression and functions of annexins in the kidney, Am. J. Physiol. Renal Physiol. 289 (2005) 949–956.
[72] K.G. Maffey, L.B. Keil, V.A. DeBari, The influence of lipid composition and divalent cations on annexin V binding to phospholipid mixtures, Ann. Clin. Lab. Sci. 31 (2001) 85–90.
[73] H. Kenis, H. van Genderen, A. Bennaghmouch, H.A. Rinia, P. Frederik, J. Narula, L. Hofstra, C.P. Reutelingsperger, Cell surface-expressed phosphatidylserine and annexin A5 open a novel portal of cell entry, J. Biol. Chem. 279 (2004) 52623–52629.
[74] S. Ravassa, A. Bennaghmouch, H. Kenis, T. Lindhout, T. Hackeng, J. Narula, L. Hofstra, C. Reutelingsperger, Annexin A5 down-regulates surface expression of tissue factor: A novel mechanism of regulating the membrane receptor repertoire, J. Biol. Chem. 280 (2005) 6028–6035.
[75] N. Gašperšič, A. Ambrožič, B. Božič, J. Majhenc, S. Svetina, B. Rozman, Annexin A5 binding to giant phospholipid vesicles is differentially affected by anti-beta2-glycoprotein I and anti-annexin A5 antibodies, Rheumatology (Oxford) 46 (2007) 81–86.
[76] B. Božič, S. Irman, N. Gašperšič, T. Kveder, B. Rozman, Antibodies against annexin A5: Detection pitfalls and clinical associations, Autoimmunity 38 (2005) 425–430.
[77] A. Cederholm, J. Frostegard, Annexin A5 in cardiovascular disease and systemic lupus erythematosus, Immunobiology 210 (2005) 761–768.
[78] J.H.W. Distler, L.C. Huber, A.J. Hueber, C.F. Reich III, S. Gay, O. Distler, D.S. Pisetsky, The release of microparticles by apoptotic cells and their effects on macrophages, Apoptosis 10 (2005) 731–741.
[79] M. Diamant, M.E. Tushuizen, A. Sturk, A.R. Nieuwland, Cellular microparticles: New players in the field of vascular disease? Eur. J. Clin. Invest. 34 (2004) 392–401.
[80] J.H.W. Distler, D.S. Pisetsky, L.C. Huber, J.R. Kalden, S. Gay, O. Distler, Microparticles as regulators of imflammation, Arthritis Rheum. 52 (2005) 3337–3348.
[81] M. Baj-Krzyworzeka, R. Szatanek, K. Weglarczyk, J. Baran, B. Urbanowicz, P. Branski, M.Z. Ratajczak, M. Zembala, Tumour-derived microvesicles carry several surface determinants and mRNA of tumour cells and transfer some of these determinants to monocytes, Cancer Immunol. Immunother. 55 (2005) 808–818.

[82] V. Kralj-Iglič, H. Hägerstrand, P. Veranič, K. Jezernik, B. Babnik, D.R. Gauger, A. Iglič, Amphiphile-induced tubular budding of the bilayer membrane, Eur. Biophys. J. 34 (2005) 1066–1070.
[83] W. Wiese, W. Harbich, W. Helfrich, Budding of lipid bilayer vesicles and flat membranes, J. Phys. Condens. Matter 4 (1992) 1647–1657.
[84] R. Lipowsky, Budding of membranes induced by intramembrane domains, J. Phys. II (France) 2 (1992) 1825–1840.
[85] A. Iglič, H. Hägerstrand, Amphiphile-induced spherical microexovesicles correponds to an extreme local area difference between two monolayers of the membrane bilayer, Med. Biol. Eng. Comput. 37 (1999) 125–129.
[86] Z. Yamashita, S.M. Masum, T. Tanaka, Y. Tamba, M. Yamazaki, Shape changes of giant unilamellar vesicles of phosphatidiylcholine induced by a *de novo* designed peptide interacting with their membrane interface, Langmuir 18 (2002) 9638–9641.
[87] M.M. Hanczyc, J.W. Szostak, Replicating vesicles as models of primitive cell growth and division, Curr. Opin. Chem. Biol. 8 (2004) 660–664.
[88] M.P. Sheetz, S.J. Singer, Biological membranes as bilayer couples. A molecular mechanism of drug-erythrocyte interactions, Proc. Natl. Acad. Sci. USA 71 (1974) 4457–4461.
[89] W. Helfrich, Blocked lipid exchange in bilayers and its possible influence on the shape of vesicles, Z. Naturforsch. 29c (1974) 510–515.
[90] E. Evans, Bending resistance and chemically induced moments in membrane bilayers, Biophys. J. 14 (1974) 923–931.
[91] W. Helfrich, Elastic properties of lipid bilayers—theory and possible experiments, Z. Naturforsch. 28c (1973) 693–703.
[92] S. Svetina, B. Žekš, Membrane bending energy and shape determination of phospholipid vesicles and red blood cells, Eur. Biophys. J. 17 (1989) 101–111.
[93] P.B. Canham, The minimum energy of bending as a possible explanation of the biconcave shape of the human red blood cell, J. Theor. Biol. 26 (1970) 61–81.
[94] A. Pralle, P. Keller, E.L. Florin, K. Simons, J.K. Horber, Sphingolipid-cholesterol rafts diffuse as small entities in the plasma membrane of mammalian cells, J. Cell Biol. 148 (2000) 997–1008.
[95] I.A. Prior, C. Muncke, R.G. Parton, J.F. Hancock, Direct visualization of Ras proteins in spatially distinct cell surface microdomains, J. Cell. Biol. 160 (2003) 165–170.
[96] P. Sharma, R. Varma, R.C. Sarasij, Ira, K. Gousset, G. Krishnamoorthy, M. Rao, S. Mayor, Nanoscale organization of multiple GPI-anchored proteins in living cell membranes, Cell 116 (2004) 577–589.
[97] S.J. Plowman, C. Muncke, R.G. Parton, J.F. Hancock, H-ras, K-ras, and inner plasma membrane raft proteins operate in nanoclusters with differential dependence on the actin cytoskeleton, Proc. Natl. Acad. Sci. USA 102 (2005) 15500–15505.
[98] K. Simons, D. Toomre, Lipid rafts and signal transduction, Nat. Rev. Mol. Cell. Biol. 1 (2000) 31–39.
[99] K. Simons, W.L. Vaz, Model systems, lipid rafts, and cell membranes, Annu. Rev. Biophys. Biomol. Struct. 33 (2004) 269–295.
[100] H. Hägerstrand, L. Mrowczynska, U. Salzer, R. Prohaska, A.K. Michelsenn, V. Kralj-Iglič, A. Iglič, Curvature dependent lateral distribution of raft markers in the human erythrocyte membrane, Mol. Membr. Biol. 23 (2006) 277–288.
[101] V. Kralj-Iglič, V. Heinrich, S. Svetina, B. Žeks, Free energy of closed membrane with anisotropic inclusions, Eur. Phys. J. B. 10 (1999) 5–8.
[102] V. Kralj-Iglič, A. Iglič, G. Gomišček, F. Sevšek, V. Arrigler, H. Hägerstrand, Microtubes and nanotubes of a phospholipid bilayer membrane, J. Phys. A: Math. Gen. 35 (2002) 1533–1549.
[103] A. Iglič, B. Babnik, K. Bohinc, M. Fošnarič, H. Hägerstrand, V. Kralj-Iglič, On the role of anisotropy of membrane constituents in formation of a membrane neck during budding of a multicomponent membrane, J. Biomech. 40 (2007) 579–585.
[104] V. Kralj-Iglič, B. Babnik, D.R. Gauger, S. May, A. Iglič, Quadrupolar ordering of phospholipid molecules in narrow necks of phospholipid vesicles, J. Stat. Phys. 125 (2006) 727–752.
[105] B. Isomaa, H. Hägerstrand, Shape transformations induced by amphiphiles in erythrocytes, Biochim. Biophys. Acta 899 (1987) 93–103.

[106] H. Hägerstrand, B. Isomaa, Morphological characterization of exovesicles and endovesicles released in human erythrocytes following treatment with amphiphiles, Biochim. Biophys. Acta 1109 (1992) 117–126.
[107] H. Hägerstrand, B. Isomaa, Lipid and protein composition of exovesicles released from human erythrocytes following treatment with amphiphiles, Biochim. Biophys. Acta 1190 (1994) 409–415.
[108] V. Kralj-Iglič, A. Iglič, H. Hägerstrand, P. Peterlin, Stable tubular microexovesicles of the erythrocyte membrane induced by dimeric amphiphiles, Phys. Rev. E 61 (2000) 4230–4234.
[109] T. Harder, K. Simons, Caveolae, DIGs, and the dynamics of sphingolipid-cholesterol microdomains, Curr. Opin. Cell Biol. 9 (1997) 534–542.
[110] D. Allan, P. Thomas, A.R. Limbrick, The isolation and characterization of 60 nm vesicles ('nanovesicles') produced during ionophore A23187-induced budding of human erythrocytes, Biochem. J. 188 (1980) 881–887.
[111] U. Salzer, P. Hinterdorfer, U. Hunger, C. Borken, R. Prohaska, Ca^{++}-dependent vesicle release from erythrocytes involves stomatin-specific lipid rafts, synexin (annexin VII), and sorcin, Blood 99 (2002) 2569–2577.
[112] J.M. Holopainen, M.I. Angelova, P.K.J. Kinnunen, Vectorial budding of vesicles by asymmetrical enzymatic formation of ceramide in giant liposomes, Biophys. J. 78 (2000) 830–838.
[113] H. Sprong, P. van der Sluijs, G. van Meer, How proteins move lipids and lipids move proteins, Nat. Rev. Mol. Cell Biol. 2 (2001) 504–513.
[114] J.C. Holthius, G. van Meer, K. Huitema, Lipid microdomains, lipid translocation and the organization of intracellular membrane transport (review), Mol. Membr. Biol. 20 (2003) 231–241.
[115] D. Tang, D. Borchman, N. Harris, S. Pierangeli, Lipid interactions with human antiphospholipid antibody, beta 2-glycoprotein 1, and normal human IgG using the fluorescent probes NBD-PE and DPH, Biochim. Biophys. Acta 1372 (1998) 45–54.
[116] S.X. Wang, G. Cai, S. Sui, Intrinsic fluorescence study of the interaction of human apolipoprotein H with phospholipid vesicles, Biochemistry 38 (1999) 9477–9484.
[117] H. Wurm, Beta 2-lycoprotein-I (apolipoprotein H) interactions with phospholipid vesicles, Int. J. Biochem. 16 (1984) 511–515.
[118] M. Igarashi, E. Matsuura, Y. Igarashi, H. Nagae, K. Ichikawa, D.A. Triplett, T. Koike, Human beta2-glycoprotein I as an anticardiolipin cofactor determined using mutants expressed by a baculovirus system, Blood 87 (1996) 3262–3270.
[119] M.I. Angelova, S. Soleau, P. Meleard, J.F. Faucon, P. Bothorel, Preparation of giant vesicles by external AC electric fields. Kinetics and applications, Prog. Colloid Polym. Sci. 89 (1992) 127–131.
[120] A. Ambrožič, B. Božič, T. Kveder, J. Majhenc, V. Arrigler, S. Svetina, B. Rozman, Budding, vesiculation and permeabilization of phospholipid membranes-evidence for a feasible physiologic role of beta2-glycoprotein I and pathogenic actions of anti-beta2-glycoprotein I antibodies, Biochim. Biophys. Acta 1740 (2005) 38–44.
[121] N. Tomšič, B. Babnik, D. Lombardo, B. Mavčič, M. Kandušer, A. Iglič, V. Kralj-Iglič, Shape and size of giant unilamellar phospholipid vesicles containing cardiolipin, J. Chem. Inf. Model. 45 (2005) 1676–1679.
[122] M. Mally, J. Majhenc, S. Svetina, B. Žekš, Mechanisms of equinatoxin II-induced transport through the membrane of a giant phospholipid vesicle, Biophys. J. 83 (2002) 944–953.
[123] E. Polz, G.M. Kostner, The binding of beta 2-glycoprotein-I to human serum lipoproteins: Distribution among density fractions, FEBS Lett. 102 (1979) 183–186.
[124] T. McNally, I.J. Mackie, D.A. Isenberg, S.J. Machin, Immunoelectrophoresis and ELISA techniques for assay of plasma beta 2-glycoprotein-I and the influence of plasma lipids, Thromb. Res. 72 (1993) 275–286.
[125] A. Ambrožič, T. Avčin, K. Ichikawa, T. Kveder, E. Matsuura, M. Hojnik, T. Atsumi, B. Rozman, T. Koike, Anti-beta(2)-glycoprotein I antibodies in children with atopic dermatitis, Int. Immunol. 14 (2002) 823–830.
[126] R. Lipowsky, The conformation of membranes, Nature 349 (1991) 475–481.

[127] A. Ambrožič, S. Čučnik, N. Tomšič, J. Urbanija, M. Lokar, B. Babnik, B. Rozman, A. Iglič, V. Kralj-Iglič, Interaction of giant phospholipid vesicles containing cardiolipin and cholesterol with β2-glycoprotein-I and anti-β2-glycoprotein-I antibodies, Autoimmun. Rev. 6 (2006) 10–15.
[128] J.D. Jackson, Classical Electrodynamics (3rd ed.), John Wiley & Sons, 1998.
[129] K. Bohinc, V. Kralj-Iglič, T. Slivnik, S. May, A. Iglič, Spatial distribution of divalent rod-like ions in contact with a charged surface, Electrotech. Rev. 73 (2006) 137–142.
[130] K. Bohinc, A. Iglič, S. May, Interaction between macroions mediated by divalent rodlike ions, Europhys. Lett. 68 (2004) 494–500.
[131] V. Kralj-Iglič, A. Iglič, A simple statistical mechanical approach to the free energy of the electric double layer including the excluded volume effect, J. Phys. II (France) 6 (1996) 477–491.
[132] D.F. Evans, H. Wennerström, The Colloidal Domain, Where Physics, Chemistry, and Biology Meet (2nd ed.), VCH Publishers, 1994.